JCB Journal of Cell Biology

ARTICLE

Spectrin couples cell shape, cortical tension, and Hippo signaling in retinal epithelial morphogenesis

Hua Deng[1], Limin Yang[2], Pei Wen[1], Huiyan Lei[1], Paul Blount[2], and Duojia Pan[1]

Although extracellular force has a profound effect on cell shape, cytoskeleton tension, and cell proliferation through the Hippo signaling effector Yki/YAP/TAZ, how intracellular force regulates these processes remains poorly understood. Here, we report an essential role for spectrin in specifying cell shape by transmitting intracellular actomyosin force to cell membrane. While activation of myosin II in *Drosophila melanogaster* pupal retina leads to increased cortical tension, apical constriction, and Yki-mediated hyperplasia, spectrin mutant cells, despite showing myosin II activation and Yki-mediated hyperplasia, paradoxically display decreased cortical tension and expanded apical area. Mechanistically, we show that spectrin is required for tethering cortical F-actin to cell membrane domains outside the adherens junctions (AJs). Thus, in the absence of spectrin, the weakened attachment of cortical F-actin to plasma membrane results in a failure to transmit actomyosin force to cell membrane, causing an expansion of apical surfaces. These results uncover an essential mechanism that couples cell shape, cortical tension, and Hippo signaling and highlight the importance of non–AJ membrane domains in dictating cell shape in tissue morphogenesis.

Introduction

During tissue morphogenesis, the spatial-temporal coordination between cell proliferation and cell shape change produces organs of proper size and shape, and disruption of this coordination is a common characteristic of developmental anomalies (Butcher et al., 2009; Halder et al., 2012; Heisenberg and Bellaïche, 2013; Huang and Ingber, 1999; Lecuit and Lenne, 2007; Nelson and Bissell, 2006). Elucidating the molecular mechanisms underlying this coordination remains a fundamental goal of developmental biology. It is now recognized that this process is mediated not only by morphogen-mediated chemical signaling but also by mechanical signals such as cell shape, cell geometry, deformation caused by the pulling forces of the extracellular matrix (ECM) and of neighboring cells, and the associated changes in cytoskeleton organization and tension, which together represent the architectural signal of a tissue (Aragona et al., 2013; Discher et al., 2009; Huang and Ingber, 1999; Nelson et al., 2005). Cells sense these mechanical cues and translate them into defined signaling responses to regulate cell behaviors such as cell proliferation and differentiation, a process termed mechanotransduction (Farge, 2011; Hoffman et al., 2011; Wozniak and Chen, 2009). Therefore, the actomyosin cytoskeleton plays a central role in mechanotransduction by generating and transmitting mechanical force in cells and has been the focus of intense studies in the past (Heisenberg and Bellaïche, 2013; Lecuit et al., 2011; Vicente-Manzanares et al., 2009). However, little is known about the roles of other types of cytoskeleton, such as the spectrin-based membrane skeleton (SBMS), in mechanotransduction (Bennett and Baines, 2001).

The tight coupling between cell shape and proliferation is a common characteristic of anchorage-dependent cells (Folkman and Moscona, 1978; Spiegelman and Ginty, 1983; Wittelsberger et al., 1981). Actomyosin cytoskeleton tension and integrity are critical for this coupling: on one hand, actomyosin contractility and reorganization cause cell shape change and regulate cell proliferation (Aragona et al., 2013; Fernández et al., 2011; Lecuit and Lenne, 2007; Sansores-Garcia et al., 2011); on the other hand, cell shape itself regulates Rho GTPase signaling to reorganize the cytoskeleton and maintain cell shape (McBeath et al., 2004). Recent studies in cultured mammalian cells have implicated YAP/TAZ, the transcriptional effectors of the Hippo signaling pathway, as key mediators of mechanotransduction through which mechanical signals regulate cell behaviors such as proliferation and survival (Dupont et al., 2011; Wada et al., 2011; Aragona et al., 2013; Zheng and Pan, 2019). A common theme emerging from these studies is that diverse mechanical signals regulate YAP/TAZ activity through a Rho-associated

[1]Department of Physiology, Howard Hughes Medical Institute, University of Texas Southwestern Medical Center, Dallas, TX; [2]Department of Physiology, University of Texas Southwestern Medical Center, Dallas, TX.

Correspondence to Duojia Pan: duojia.pan@utsouthwestern.edu.

protein kinase (Rok)–nonmuscle myosin II (hereafter myosin II) pathway that impinges on actomyosin contractility. However, these studies often involved manipulating external forces or ECM stiffness to cause stretching or compression of cells, which is different from tissue morphogenesis where cell shape changes are mainly driven by cell-intrinsic forces. Indeed, while manipulating external forces or ECM stiffness in cultured mammalian cells revealed a positive correlation between cell area and YAP/TAZ activity (Aragona et al., 2013; Puliafito et al., 2012), increasing cortical tension cell intrinsically in intact epithelia resulted in Yki activation accompanied by decreased cell area (apical constriction; Deng et al., 2015), At present, the molecular mechanisms that couple cell shape, cortical tension, and Hippo signaling in intact epithelia remain poorly understood.

The prevailing paradigm of cell shape regulation in tissue morphogenesis suggests that cell shape is largely governed by two antagonistic forces: an E-cadherin–mediated adhesion force that stabilizes cell contacts, and cell cortical tension exerted by the actomyosin network that tends to reduce cell–cell interface (Fig. 1 A; Lecuit and Lenne, 2007; Rauzi and Lenne, 2011). The antagonistic interplay of these two forces produces the intercellular surface tension that dictates cell–cell interaction according to the principle of energy minimization (Heisenberg and Bellaïche, 2013). Mechanistically, it is believed that this interplay is mediated by adherens junctions (AJs) where E-cadherin organizes the cortical actomyosin network through α-catenin and its associated proteins, (Fig. 1 A; Harris and Tepass, 2010; Lecuit and Yap, 2015; Priya and Yap, 2015). According to this model, contraction force generated by actomyosin is transferred to cell plasma membrane through AJs to effect cell shape change. This model was recently challenged by findings that in embryonic cells undergoing apical constriction during *Drosophila melanogaster* gastrulation, the cell shape changes follow the contraction pulse of the apical-medial cortical actomyosin, not the actomyosin belt linked with AJs (Coravos and Martin, 2016; Martin et al., 2009). These findings raised two interesting questions: does non–AJ-associated cortical actomyosin regulate cell shape in other epithelia such as imaginal discs? How is non–AJ-associated cortical actomyosin linked to plasma membrane?

Spectrin is a large, springlike protein that forms the SBMS beneath the plasma membrane by cross-linking short F-actin and binding integral membrane proteins (Bennett and Baines, 2001; Machnicka et al., 2012; Pinder and Baines, 2000). *Drosophila* encodes one spectrin α subunit (α-Spec) and two spectrin β subunits (β-Spec and βHeavy-spec [βH-Spec]), which generate two spectrin tetramers, $(\alpha\beta)_2$ and $(\alpha\beta H)_2$. In *Drosophila* ovarian follicle and imaginal epithelial cells, β-Spec and βH-Spec are localized to the lateral and apical membrane, respectively, while α-Spec is localized along the entire apical-basal axis (Deng et al., 2015; Lee et al., 1997). Recent studies from several groups showed that spectrin is a tumor suppressor and regulates cell proliferation through Hippo signaling (Deng et al., 2015; Fletcher et al., 2015; Wong et al., 2015). Our work in particular suggested that spectrin regulates Hippo signaling by modulating cortical actomyosin activity, since loss of spectrin results in elevated cortical myosin II activity that activates Yki and causes cell overproliferation (Deng et al., 2015). In our continued characterization of spectrin function, we found that unlike wild-type imaginal disc cells, in which internal activation of myosin II leads to apical constriction and increased cortical tension coupled with Yki activation, spectrin mutant cells, despite showing myosin II and Yki activation, display decreased cortical tension and expanded apical area. Thus, cell shape and cortical tension can be uncoupled from Yki activity in the absence of spectrin. Mechanistically, we show that spectrin is required to attach cortical F-actin to cell membrane domains outside the AJs. This function is critical for transmitting actomyosin force to cell membrane and thus dictating cell shape in tissue morphogenesis. These findings uncover an essential mechanism that couples cell shape, cortical tension, and Hippo signaling in intact tissues.

Results

The coupling between cell shape and Yki-mediated cell proliferation is disrupted in spectrin mutant cells

The simplicity of the developing *Drosophila* retina has made it an especially useful model for studying epithelial morphogenesis (Cagan and Ready, 1989; Carthew, 2007). The *Drosophila* retina is an epithelium composed of a hexagonal array of repeating functional units called ommatidia. Each ommatidium has a neuronal core of 8 photoreceptors and 4 cone cells surrounded by 11 light-insulating pigment epithelial cells (PECs; Fig. 1 B). By 40 h after puparium formation (APF), each type of PEC (two primary [1°] PECs, six secondary [2°] PECs, and three tertiary [3°] PECs) has adopted a unique and precise morphology repeated across all ommatidia (Fig. 1 B). This allows changes in PEC morphology to be easily detected, quantified, and structurally analyzed. Moreover, the number of interommatidial cells (including six 2° PECs, three 3° PECs, and three bristle cells; Fig. 1 B), which is exquisitely sensitive to Hippo signaling, provides an easily quantifiable measure of cell proliferation (Hamaratoglu et al., 2006; Yu and Pan, 2018). Since many genes analyzed in this study have essential function in earlier development, we relied on clonal analyses in pupal retina to interrogate the molecular mechanisms coordinating cell shape and Yki activity (all pupal eyes were analyzed ∼40 h APF unless otherwise indicated). Given that α-Spec is the major component of both apical and lateral SBMS in the epithelial cells, we focused our analysis on *α-spec*. For the reader's convenience of following mosaic genotypes in the figures, color-coded letters are used to indicate mutant versus wild-type cells that were experimentally marked by the corresponding colors.

We first examined how cell shape is regulated by cortical tension in *Drosophila* retina morphogenesis. Cell cortical tension is produced by the actomyosin cytoskeleton, whose major components are myosin II and F-actin (Fig. 1 A; Lecuit et al., 2011). As the major force generator in most cell types, the activity of myosin II is regulated by phosphorylation of myosin light chain (MLC) by multiple kinases including Rok (Vicente-Manzanares et al., 2009). Phosphorylation of MLC greatly increases the Mg^{2+}-ATPase activity of myosin in the presence of actin and leads to the generation of contractile forces or tension (Somlyo and Somlyo, 2003). Spaghetti squash (Sqh) is the *Drosophila* homology of MLC and a constitutively active Sqh mutant,

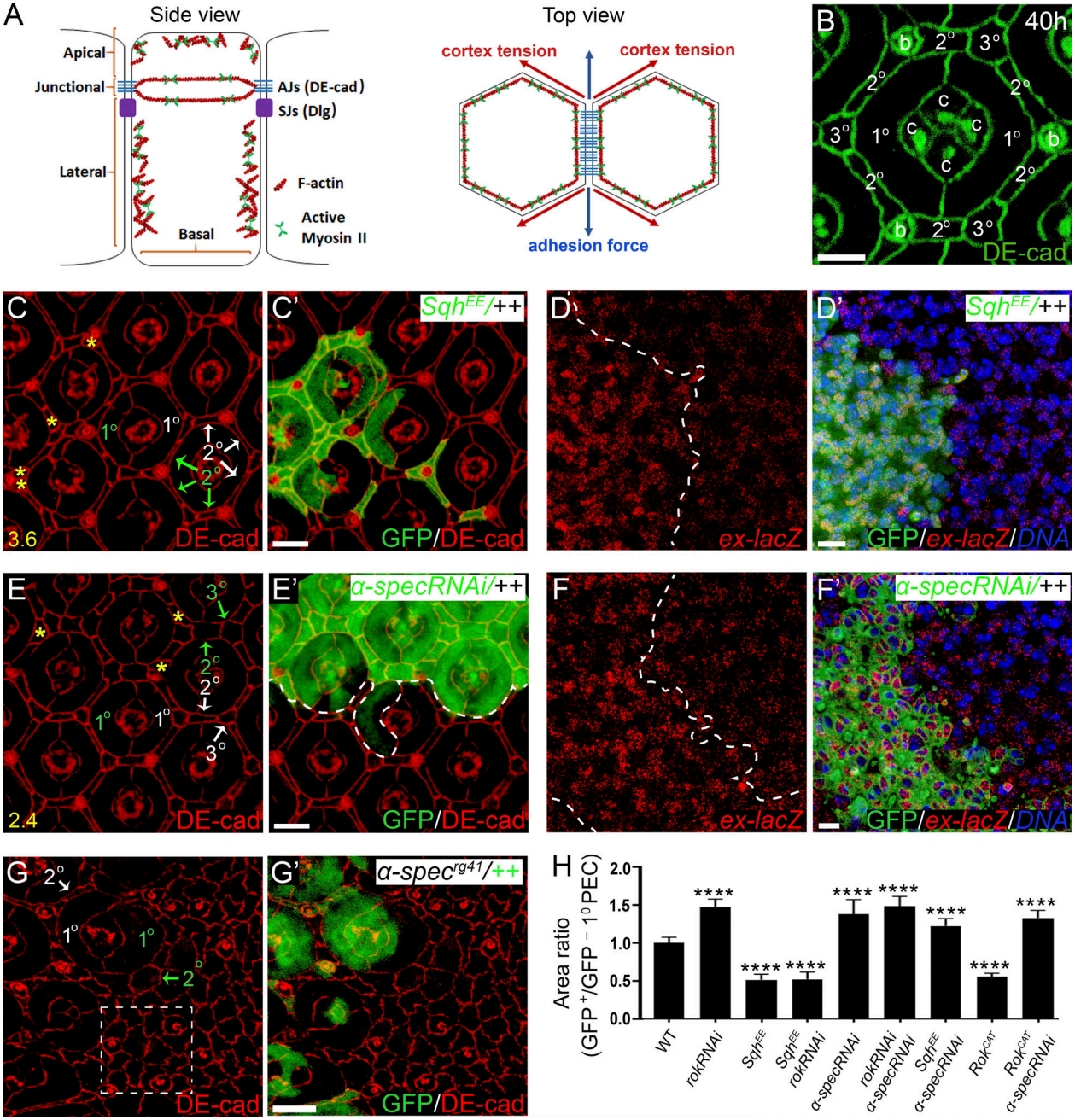

Figure 1. **Spectrin couples cell shape and Hippo signaling in *Drosophila* retina development. (A)** A cartoon showing side view (cross section) and top view (tangential section around AJs) of imaginal disc epithelial cells. Left (side view): The apical membrane domain includes the membrane region above the AJs; the lateral membrane domain includes the membrane region below the AJs but not the basal membrane that faces the ECM; junctional membrane domain refers to AJ-associated membrane region. Note the AJ-associated actomyosin cytoskeleton attached to membrane through AJs, and the apical and lateral cortical actomyosin cytoskeleton attached to the membrane. The septate junctions (SJs) containing Dlg are located laterally to AJs. Right (top view): Cell shape is dictated by cell surface tension, which is determined by the antagonistic cortical tension and adhesion force. **(B)** DE-cad staining highlighting the hexagonal geometry of a single wild-type pupal eye ommatidium at 40 h APF. The four cone cells (c), two 1° PECs, six 2° PECs, three 3° PECs, and three bristle cells (b) of an ommatidium are marked. **(C and C')** A pupal eye disc containing GFP-positive MARCM clones with Sqh^{EE} overexpression was stained for DE-cad. PECs with Sqh^{EE} overexpression (green labels in C) exhibit decreased apical size compared with the corresponding wild-type PECs (white labels in C) in the same ommatidium. Also note the extra interommatidial cells (yellow asterisks in C) in ommatidia with Sqh^{EE} overexpression. 20 ommatidial clusters were used for counting interommatidial cells, and the number on the lower left in C indicates the number of extra cells per cluster. **(D and D')** A pupal eye disc containing GFP-positive clones with Sqh^{EE} overexpression was stained for *ex-lacZ* and DNA dye DAPI. Note the elevated *ex-lacZ* level in clones with Sqh^{EE} overexpression. **(E and E')** A pupal eye disc containing GFP-positive MARCM clones with *α-spec* RNAi was stained for DE-cad. PECs with *α-spec* RNAi (green labels in E) exhibit increased apical size compared to the corresponding wild-type PECs (white labels in E) in the same ommatidium. Also note the extra interommatidial cells (yellow asterisks in E) in ommatidia with *α-spec* RNAi. 20 ommatidia were used for counting interommatidial cells, and the number on the lower left in E indicates the number of extra cells per cluster. **(F and F')** A pupal eye disc containing GFP-positive MARCM clones with *α-spec* RNAi was stained for *ex-lacZ* and DNA dye DAPI. Note the elevated *ex-lacZ* level in clones with *α-spec* RNAi. **(G and G')** A pupal eye disc containing GFP-negative $\alpha\text{-spec}^{rg41}$ mutant clone was

stained for DE-cad. *α-spec*^{rg41} mutant PECs (green labels in G) exhibit increased apical size compared with the corresponding wild-type PECs (white labels in G) in the same ommatidium. Also note the absence of the hexagonal geometry of the mutant ommatidium (dashed line boxed region in G) compared with the wild-type ommatidium (B). **(H)** Quantification of apical area of the indicated mutant 1° PEC relative to the corresponding wild-type 1° PEC in the same ommatidium (means ± SEM, *n* = 15 for each genotype), ****, P < 0.0001 (Student's *t* test, all compared with wild type). Scale bars, 3 µm (B), 5 µm (C', D', E', F', and G').

Sqh^{EE}, mimics phosphorylated Sqh at Thr20 and Ser21 by replacing these residues with glutamate (Winter et al., 2001).

We focused our analysis on 1° PECs due to their large size and the convenience of comparing two 1° PECs of different genotypes side by side within a single mosaic ommatidium, although 2° and 3° PECs show similar shape change (Fig. 1 and Fig. S1). Consistent with previous studies (Warner and Longmore, 2009a, 2009b), increasing cortical tension internally by overexpressing Sqh^{EE} or an active form of Rok (Rok^{CAT}; Winter et al., 2001) caused cells to shrink their apical area, which was most obvious in 1° PECs (Fig. 1, C–C'; and Fig. S1, A–A'''). Accompanying this cell shape change, increased cortical tension also produced supernumerary interommatidial cells (Fig. 1 C and Fig. S1 A''), suggesting Yki activation. Indeed, the expression of *expanded-lacZ* (*ex-lacZ*), a well-characterized Hippo signaling reporter, was upregulated in clones with Sqh^{EE} overexpression (Fig. 1, D–D'). This result highlights an actomyosin-mediated coupling between cell shape change and Yki-mediated cell proliferation during *Drosophila* retina morphogenesis. Paradoxically, we found that PECs with *α-spec* RNAi showed enlarged apical area, despite having an elevated level of cortical myosin II activity (Deng et al., 2015), hyperplasia, and Yki activation (Fig. 1, E–F'). A similar enlargement of apical area was observed in *α-spec*^{rg41} null mutant PECs (Fig. 1, G–G'), which also lost their characteristic cell shape and hexagonal geometry of pupal ommatidia (compare Fig. 1 G with Fig. 1 B). Importantly, *α-spec* RNAi PECs show normal apical-basal polarity as revealed by PAR-3 and discs large (Dlg) staining (Fig. S2, A–B'''), suggesting that the apical enlargement of spectrin mutant PECs is unlikely to be caused by a general cell polarity defect. Furthermore, the apical surface area of ommatidium in which all cells expressed *α-spec* RNAi was larger than fully wild-type ommatidia (Fig. S2, C–E), supporting that the increased apical area of mutant PECs we observed in mosaic *α-spec* RNAi ommatidia represents a cell-autonomous defect.

We noted that *α-spec* RNAi PECs also showed an enlarged tangential area at the level of the Dlg-positive lateral domain (Fig. S2, A–A''' and E), while *β-spec*^{C} null mutant PECs showed enlargement of lateral but not apical area (Fig. S2, F–H). These findings are consistent with the relative subcellular localization of α- and β-Spec along the apical-basal axis (Deng et al., 2015; Lee et al., 1997). We infer from these observations that loss of spectrin somehow compromises the coupling between myosin II activity, cell shape, and Yki activation. Consistent with this hypothesis, when the cortical myosin II activity in 1° PECs with *α-spec* RNAi was further enhanced by overexpressing Sqh^{EE} or Rok^{CAT}, the mutant PECs still showed apical expansion (Fig.1 H and Fig. S1, H–I'). The failure of spectrin mutant PECs to respond to myosin II activation (Fig. 1 H and Fig. S1) suggests a potential explanation for the cell shape and packing defect in spectrin mutant PECs: in the absence of spectrin, myosin II activity cannot be transmitted to establish the proper intercellular surface tension, thereby causing defects in cell shape and cell packing. We also infer from these results that cell shape per se is not a determinant of Yki activity, as both apical constriction and expansion in the same cell type can be coupled to Yki activation depending on the presence or absence of spectrin.

Spectrin mediates the tight association of cortical actomyosin with plasma membrane domains outside of AJs

We considered two possible explanations for the cell shape defects of spectrin mutant PECs. First, despite elevated myosin II activity, actin polymerization may be compromised in spectrin mutant PECs such that the overall actomyosin function is compromised. Indeed, spectrin has been reported to regulate cortical actin polymerization in mammalian cells through its interaction with the F-actin elongation factors enabled (Ena)/VASP (Benz et al., 2008, 2013; Krause et al., 2003). However, we did not observe visible changes in the level or localization of the *Drosophila* Ena/VASP orthologue Ena, in spectrin mutant PECs (Fig. S2, I–J). Furthermore, even a null mutation in Ena (*ena*^{46}) did not cause any detectable changes in cortical F-actin, as revealed by phalloidin staining in Triton X-100–permeabilized pupal eye discs (Fig. S2, K–L). We therefore examined the alternative possibility that spectrin may be required for tethering cortical F-actin to cell membrane such that loss of spectrin compromises the transmission of actomyosin contraction force to cell membrane and causes abnormal cell shape.

To examine this hypothesis, we first visualized cortical F-actin in nondetergent-permeabilized pupal eye discs with a commonly used GFP reporter containing actin binding domain of utrophin (utABD-GFP; Burkel et al., 2007). We observed normal cortical F-actin levels in spectrin mutant clones compared with neighboring wild-type cells (Fig. 2, A–B' and F), suggesting that actin polymerization per se is not compromised in spectrin mutant PECs. Interestingly, when F-actin was visualized by phalloidin staining in Triton X-100–permeabilized pupal eye discs, we observed a dramatic decrease of cortical F-actin levels in spectrin mutant PECs compared with wild-type PECs (Fig. 2, C–D' and G), suggesting that the strong interaction between cytoskeleton and plasma membrane, which is normally resistant to solubilization by Triton X-100 (Doherty and McMahon, 2008; Kapus and Janmey, 2013), is compromised. Taken together, these findings suggest that spectrin is required not for actin polymerization per se but rather for the tight association of cortical F-actin to cell membrane. To further corroborate this idea, we expressed a membrane-targeted mCD8-GFP-utABD fusion protein in spectrin mutant PECs as a way of constitutively attaching F-actin directly to cell membrane, independent of spectrin. Indeed, this fusion protein resulted in accumulation of cortical F-actin that was resistant to removal by Triton X-100 in spectrin mutant PECs (Fig. 2, E–E''').

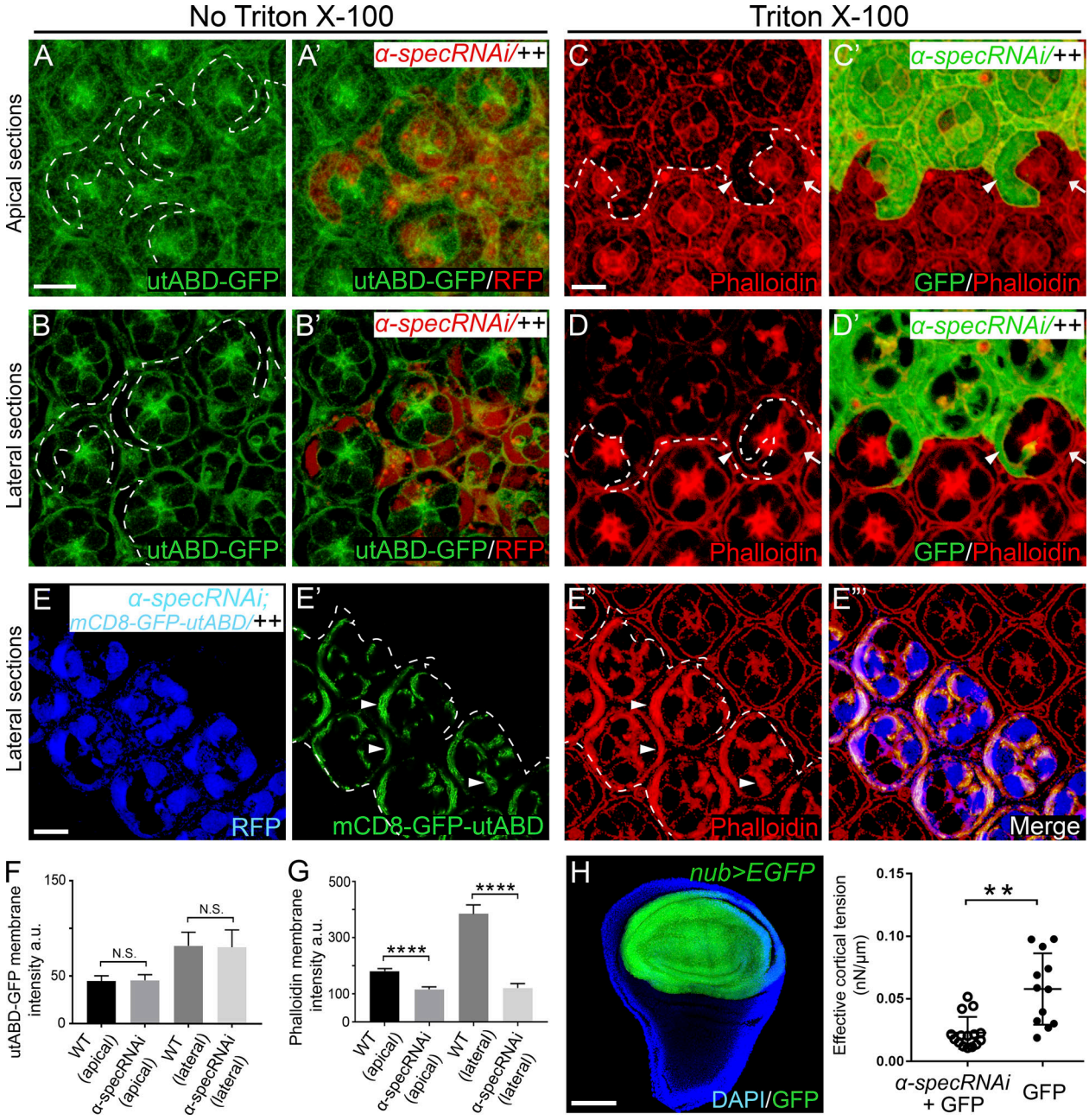

Figure 2. **Spectrin is required for attaching cortical F-actin to the cell membrane. (A–B')** A nonpermeabilized pupal eye disc containing RFP-positive MARCM clones with *α-spec* RNAi was imaged for utABD-GFP at the indicated apical-basal positions. Note normal cortical F-actin in *α-spec* mutant PECs. Quantification of utABD-GFP membrane intensity is shown in F. **(C–D')** A Triton X-100–permeabilized pupal eye disc containing GFP-positive MARCM clones with *α-spec* RNAi was stained for phalloidin. C and C' and D and D' show z-projections around cell apical and lateral plane, respectively. Note the reduced cortical F-actin level in *α-spec* mutant PECs (arrowheads) in both apical and lateral membrane compared with wild-type PECs (arrows). Quantification of phalloidin membrane intensity is shown in G. **(E–E"')** A Triton X-100–permeabilized pupal eye disc containing RFP-positive MARCM clones with *α-spec* RNAi and mCD8-GFP-utABD expression was imaged for mCD8-GFP-utABD and stained for phalloidin. Note the strong cortical F-actin staining in cell cortex where mCD8-GFP-utABD accumulated (arrowheads in E' and E"). **(F)** Quantification of mean utABD-GFP intensity in the specified membrane domains analyzed in A–B'. Note no significant difference between *α-spec* mutant PECs and wild-type PECs. Data are means ± SEM ($n \geq 20$ cells, representative of 10 pupal eyes); N.S., no significance (Student's *t* test). **(G)** Quantification of mean phalloidin intensity in the specified membrane domains analyzed in C–D'. Note significant decrease of phalloidin membrane intensity in *α-spec* mutant PECs. Data are means ± SEM ($n \geq 20$ cells, representative of 10 pupal eyes). ****, $P < 0.0001$. **(H)** Reduced cortical tension in spectrin mutant cells. Left: A *nub-Gal4 UAS-EGFP* driver showing EGFP expression in the wing pouch region in third instar wing discs. Right: Measurement of cortical tension by MPA. The Teff was measured for individual cells of the indicated genotype and plotted in the graph (means ± SEM, $n = 15$ for spectrin mutant cells, $n = 12$ for control cells). **, $P < 0.01$ (Student's *t* test). Scale bars, 5 μm (A, C, and E) and 100 μm (H).

Taken together, we suggest that the cell shape defects of spectrin mutant PECs are caused by the loss of tight association of cortical F-actin to plasma membrane, which compromises the transmission of actomyosin contraction force to cell membrane and therefore results in their apical expansion.

Our model predicts that in the absence of spectrin, the failure to transmit actomyosin force to cell membrane would result in decreased cortical tension (i.e., softer cells), despite increased myosin II activity in spectrin mutant cells. We tested this prediction by directly measuring cortical tension. To do so, a *nub-Gal4 UAS-EGFP* driver was used to knockdown *α-spec* specifically in the pouch region of wing imaginal discs (Fig. 2 H). The resulting wing discs were digested, and individual EGFP-labeled spectrin mutant or control cells were isolated and measured for cortical tension using the micropipette aspiration (MPA) technique (Kee and Robinson, 2013). As predicted by our model, the spectrin mutant cells were indeed softer than control cells (Fig. 2 H). These results further support a critical role for spectrin in transmitting actomyosin force to cell membrane.

Loss of spectrin does not affect the attachment of AJ-associated F-actin to cell membrane or transmission of cortical force to AJs

It is generally believed that the interplay between cell–cell adhesion and cell cortical tension is mediated through AJs and AJ-associated actomyosin (Lecuit and Yap, 2015; Ratheesh and Yap, 2012). To examine whether the AJs and AJ-associated actomyosin are affected in spectrin mutant PECs, we costained F-actin with *Drosophila* E-cadherin (DE-cad), a major component of AJs. Interestingly, spectrin mutant PECs showed no detectable changes in DE-cad staining; additionally, the AJ-associated F-actin cables were normally associated with cell membrane in spectrin mutant PECs in Triton X-100–permeabilized pupal eye discs, despite showing reduced cortical F-actin in the non-AJ membrane domain (Fig. 3, A–A‴ and E). The normal AJ-associated F-actin cables, along with the elevated cortical myosin II activity in spectrin mutant PECs, suggest that AJs may be under higher tension in spectrin mutant PECs due to the unaffected transmission of cortical force to AJs. In agreement with this prediction, the LIM protein Jub and its binding partner Warts (Wts), which are known to accumulate in response to tension at AJs (Rauskolb et al., 2014), accumulated to higher level at AJs in spectrin mutant PECs compared with wild-type PECs (Fig. 3, B–C′). This increased accumulation of Jub and Wts to AJs caused inhibition of Wts activity, leading to Yki activation, as shown by the up-regulation of Ex level in spectrin mutant PECs (Fig. 3, D and D′). We note that the increased accumulation of Jub and Wts to AJs in spectrin-depleted pupal eyes differs from what we reported previously in third instar wing discs, where no obvious accumulation of Jub and Wts to AJs was observed in spectrin mutant cells (Deng et al., 2015), likely due to the different sensitivity of cells to cortex tension in different tissue types and/or developmental stages. Taken together, our results suggest that spectrin is specifically required to attach F-actin to cell membrane domains outside the AJs in the pupal eyes. Furthermore, given the numerous studies demonstrating that higher tension at the AJs leads to cell constriction (Lecuit and Lenne, 2007; Lecuit and Yap, 2015; Warner and Longmore, 2009a), our findings highlight the importance of non–AJ-associated cortical tension in controlling cell shape, as decreased cortical tension outside the AJs leads to cell expansion despite higher tension at the AJs in spectrin mutant PECs.

Adducin is required for recruiting α-Spec to cell cortex and loss of adducin phenocopies spectrin mutant cells

To function as an essential linkage between F-actin and cell membrane, spectrin should physically interact with both molecular entities. Indeed, both β-spec and βH-Spec contain a weak actin binding domain, and spectrin–actin interaction is further enhanced by the membrane skeleton protein adducin (Bennett et al., 1988; Gardner and Bennett, 1987; Li et al., 1998). This prompted us to examine the potential role of the single adducin orthologue in *Drosophila*, encoded by the *hu-li tai shao* (*hts*) gene (Yue and Spradling, 1992), in anchoring F-actin to cell membrane. As in spectrin mutant PECs, the cortical F-actin was decreased in hts^{null} mutant PECs, most prominently in the Dlg-positive lateral area, in Triton X-100–permeabilized pupal eye discs (Fig. 4, A, A′, and H; and Fig. S3, A–B′ and E). These results are consistent with the established role of adducin in facilitating the interactions between spectrin and F-actin.

Interestingly, we found that cortical spectrin was significantly decreased in hts^{null} mutant PECs, as revealed by antibody staining (Fig. 4, B, B′, and I) or a GFP–α-Spec fusion protein (Fig. 4, C, C′, and J). On the other hand, loss of spectrin did not affect the cortical localization of Hts as revealed by a GFP–Hts fusion protein (Fig. 4, D, D′, and K). Thus, Hts is required for the cortical localization of spectrin. Consistent with adducin and spectrin functioning in a common pathway, hts^{null} mutant PECs showed increased level of cortical phosphorylated MLC (p-MLC; Fig. 4, E, E′, and L) as well as supernumerary interommatidial cells (Fig. 4, F and G), with both phenotypes resembling those observed in spectrin mutant PECs (Deng et al., 2015). We noted that, unlike *α-spec* mutant PECs, which showed enlargement of both apical and lateral areas, hts^{null} mutant PECs showed enlargement of lateral area only (Fig. S3, C–D′ and F). The lack of apical enlargement in hts^{null} mutant PECs is likely due to the remaining level of apical cortex F-actin in these mutant cells (~80% compared with wild-type control), which is significantly higher than that in *α-spec* mutant PECs (~60% compared with wild-type control; Fig. S3 G).

The Pleckstrin homology (PH) domain of β-Spec mediates the interaction of spectrin with the cell membrane in *Drosophila* retina

Previous studies in human red blood cells have implicated the membrane-associated protein 4.1 and Ankyrin (Ank) in recruiting spectrin to plasma membrane (Bennett and Baines, 2001). However, little is known about how spectrin interacts with plasma membrane in epithelial cells. *Drosophila* contains a single orthologue of protein 4.1 named *cora* and two homologues of Ank called Dank1 and Dank2, with Dank2 expressed in neurons only. In contrast to what has been reported in human red blood cells (Bennett and Baines, 2001), we did not observe reduced cortical α-Spec level in $cora^{5}$ null mutant cells (Fig. S4, A,

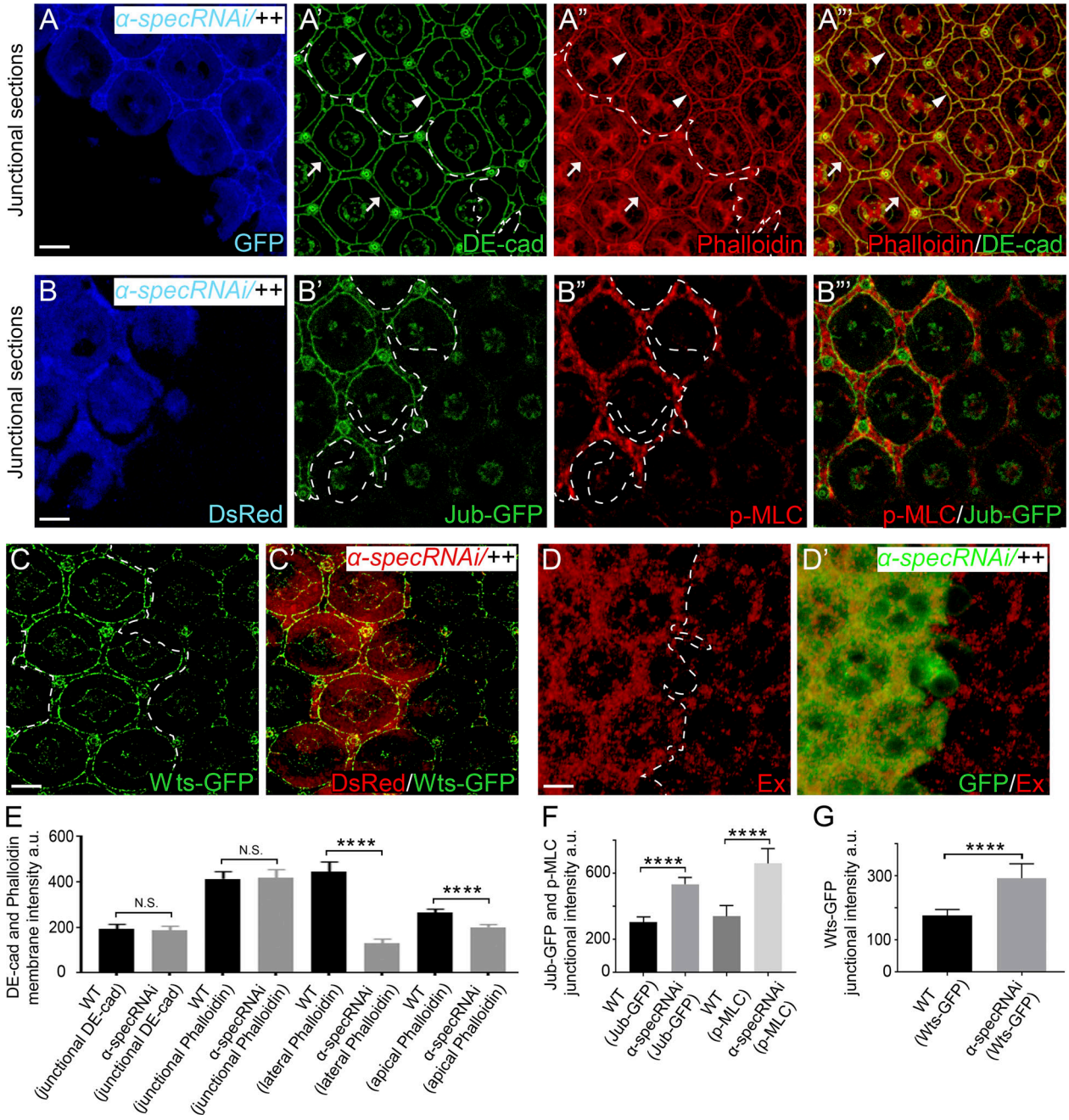

Figure 3. **Spectrin is not required for attaching AJ-associated F-actin to cell membrane or transmission of cortical force to AJs. (A–A"')** A Triton X-100–permeabilized pupal eye disc containing GFP-positive MARCM clones with *α-spec* RNAi was stained for the AJ marker DE-cad and phalloidin. Note the normal DE-cad and circumferential F-actin cables associated with AJs in *α-spec* mutant PECs (arrowheads in A'–A"') compared with those in the neighboring wild-type PECs (arrows in A'–A"'). Quantification of DE-cad and phalloidin intensity is shown in E. **(B–B"')** A pupal eye disc containing DsRed-positive clones with *α-spec* RNAi was imaged for Jub-GFP and stained for p-MLC. Note the increased level of Jub-GFP at AJs (B') and increased cortical p-MLC (B") in *α-spec* mutant PECs. Quantification of Jub-GFP and p-MLC junctional intensity is shown in F. **(C and C')** Similar to B–B"' except that Wts-GFP was examined. Note the increased level of Wts-GFP in *α-spec* mutant PECs (C). Quantification of Wts-GFP junctional intensity is shown in G. **(D and D')** A pupal eye disc containing GFP-positive MARCM clones with *α-spec* RNAi was stained for Ex. Note the elevated Ex level in clones with *α-spec* RNAi. **(E–G)** Quantification of mean membrane intensity of the indicated proteins in the specified membrane domains. Data are means ± SEM ($n \geq 20$ cells, representative of 10 pupal eyes). ****, $P < 0.0001$. Scale bars, 5 µm. N.S., no significance.

A', and E) or *Dank1* RNAi cells (Fig. S4, B, B', and F). To the contrary, α-Spec level was increased in *cora*^{5} mutant cells (Fig. S4, A, A', and E). These findings suggesting that neither Cora nor Dank1 is required for recruiting spectrin to the cell membrane in *Drosophila* retina epithelia.

The β-Spec or βH-Spec subunit contains a PH domain. Since PH domains are known to bind phospholipids in the plasma membrane (Lemmon, 2008), we examined whether the PH domain of β-Spec is required for recruiting spectrin to cell membrane. Like *α-spec* mutant PECs, *β-spec*^{C} null mutant PECs

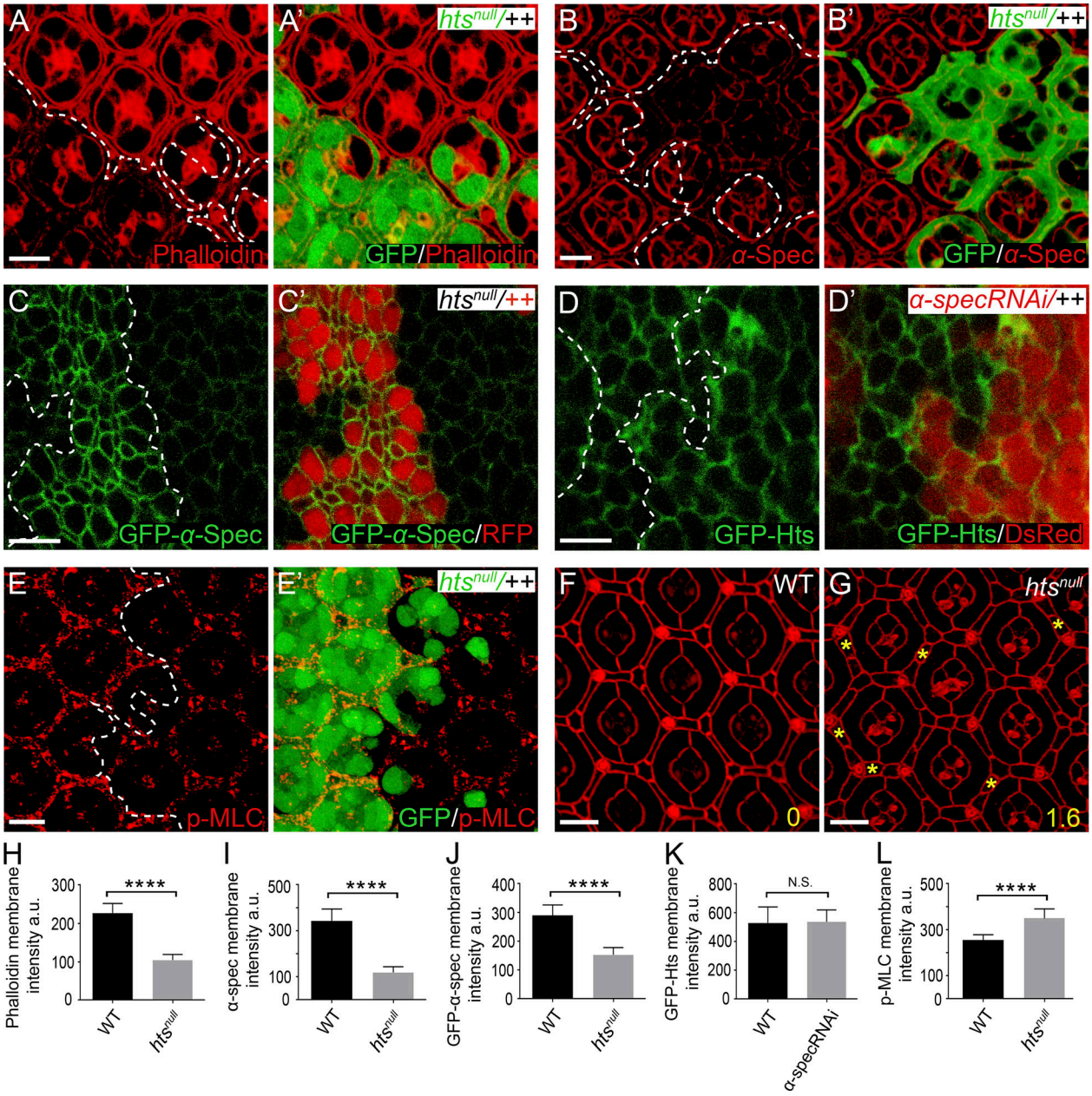

Figure 4. **Hts is required for recruiting α-Spec to cell cortex and loss of Hts phenocopies spectrin mutants.** The z-projections at lateral domain (A–E) and AJs (F and G), respectively. **(A and A')** A Triton X-100–permeabilized pupal eye disc containing GFP-positive *hts*^{null} MARCM clones was stained for phalloidin. Decreased cortical F-actin level in *hts*^{null} mutant PECs was most obvious in lateral domain (A and A') but less obvious in apical domain (see Fig. S3, A and A'). Quantification of phalloidin membrane intensity is shown in H. **(B and B')** Similar to A and A' except that α-Spec staining is shown. Note the decreased cortical α-Spec level in *hts*^{null} mutant PECs. Quantification of α-Spec membrane intensity is shown in I. **(C and C')** A third instar wing disc containing RFP-negative *hts*^{null} mutant clones was imaged for GFP–α-Spec. Note the dramatically decreased level of cortical GFP–α-Spec in *hts*^{null} mutant clones. Quantification of GFP–α-Spec membrane intensity is shown in J. **(D and D')** A third instar wing disc containing DsRed-positive clones expressing *α-spec* RNAi was imaged for GFP-Hts. Note the similar level of cortical GFP-Hts inside and outside the mutant clones. Quantification of GFP-Hts membrane intensity is shown in K. **(E and E')** A pupal eye disc containing GFP-positive MARCM clones with the *hts*^{null} mutation was stained for p-MLC. Note the increased level of cortical p-MLC in the *hts*^{null} mutant cones. Quantification of p-MLC membrane intensity is shown in L. **(F and G)** Pupal eye discs of the indicated genotypes were stained for DE-cad. Note the extra interommatidial cells in *hts* mutant eye discs (yellow asterisks in G). 20 ommatidia of each genotype were used for counting interommatidial cells, and the number on the lower right of each panel indicates the number of extra cells per cluster. **(H–L)** Quantification of mean membrane intensity of the indicated proteins analyzed in A–E. Data are means ± SEM ($n \geq 20$ cells, representative of five animals). ****, $P < 0.0001$. Scale bars, 5 µm. N.S., no significance.

also showed decreased lateral cortex F-actin staining in Triton X-100–permeabilized pupal eye discs (Fig. 5, A–B). We found that a β-Spec mutant lacking the PH domain (β-SpecΔPH) not only failed to localize to the cell membrane but also failed to rescue the cortical F-actin or the lateral enlargement phenotypes in *β-spec*^{C} mutant PECs (Fig. 5, B–C"'; and Fig. S4, C, C', and G). By contrast, these defects were rescued by a fusion protein containing β-SpecΔPH and a membrane-targeting myristoylation signal (Myr-β-SpecΔPH; Fig. 5, B and D–D"'; and Fig. S4, D, D', and G). As expected, both wild-type and a β-Spec mutant missing the Ank-binding domain (β-Spec$^{\alpha 8}$) were properly localized to the cell membrane and fully rescued the *β-spec*^{C} mutant phenotypes (Fig. 5, B and E–F"'). These results highlight the importance of PH domain–mediated interactions, but not Ank binding, in membrane localization and function of spectrin in *Drosophila* retina epithelial cells.

Arp2/3-initiated actin polymerization incorporates spectrin into the cortical actomyosin network

We noted that *α-spec* RNAi mutant PECs still showed some residual cortical F-actin in the presence of Triton X-100 (Fig. 2, C–D'). This suggests that there are distinct pools of cortical F-actin, and only some of them are attached to cell membrane in a spectrin-dependent manner. Indeed, cortical actomyosin cytoskeleton is a complex network regulated by many different actin polymerization factors (Campellone and Welch, 2010; Pollard and Borisy, 2003). To understand how this complex network interacts with spectrin, we changed F-actin dynamics by manipulating several major regulators of actin polymerization, including Arp2/3 complex (Goley and Welch, 2006), capping protein (CP; Edwards et al., 2014), and diaphanous (Dia; Pollard, 2007). Interestingly, promoting Arp2/3-mediated actin polymerization, through the expression of a membrane-targeted Wiskott–Aldrich syndrome protein containing a myristoylation signal (Myr-WASp; Bertet et al., 2009; Takenawa and Suetsugu, 2007), resulted in increased cortical F-actin and spectrin level (Fig. 6, A–B', F, and G). Conversely, mutant cells lacking the Arp2/3 component Arpc1 showed decreased cortical spectrin level (Fig. 6, E and E'). By contrast, loss of the CP subunit Cpa or overexpression of constitutively active Dia (Dia^{CA}) did not increase cortical spectrin level (Fig. S4, H–K). We infer from these observations that spectrin specifically interacts with Arp2/3-initiated F-actin, but not CP- or Dia-regulated F-actin, in the cell cortex. Such specificity provides a potential explanation for the residual (i.e., spectrin-independent) F-actin attachment to cell membrane observed in spectrin mutant PECs.

Since adducin preferentially recruits spectrin to the fast-growing ends of actin filament in vitro (Li et al., 1998), we examined whether Hts is involved in the incorporation of spectrin to the growing F-actin initiated by Arp2/3. Indeed, the increased cortical F-actin and spectrin resulting from Myr-WASp overexpression disappeared in *hts*^{null} mutant PECs (Fig. 6, C–D', F, and G). Thus, in the cell cortex, spectrin is incorporated into the growing F-actin initiated by Arp2/3 in a Hts-dependent manner. Taken together with the requirement of spectrin in tethering F-actin to cell membrane, these results uncover a feed-forward mechanism for anchoring spectrin-based and the actin-based cytoskeletons to cell membrane domains outside of AJs.

The failure to transmit actomyosin force to cell membrane in spectrin mutant cells can be rescued by inactivation of *cpa*

The results presented so far suggest the existence of distinct pools of cortical F-actin, some of which are attached to cell membrane in a spectrin-dependent manner. Furthermore, defects in spectrin-mediated attachment of F-actin to cell membrane compromise the transmission of actomyosin tension, resulting in aberrant cell shape. To examine the functional interplay (if any) between spectrin-dependent and -independent F-actin pools in force transmission, we investigated whether increasing the spectrin-independent F-actin pools may compensate for the loss of spectrin-dependent F-actin pool in dictating cell shape. We tested this possibility by increasing F-actin levels through the inactivation of the CP subunit Cpa, since this pool of F-actin does not appear to interact with spectrin, as shown above (Fig. S4, H–I). As expected, *cpa* RNAi resulted in increased cortical F-actin (Fig. 7, A, A', and F). Moreover, in Triton X-100–permeabilized pupal eye discs, *cpa* RNAi restored cortical F-actin in spectrin mutant PECs to a level higher than that in wild-type PECs (Fig. 7, B, B', and F), demonstrating that loss of Cpa sufficed to restore appropriate F-actin attachment to cell membrane in spectrin mutant PECs. Importantly, along with the rescue of F-actin attachment to cell membrane, *cpa* RNAi also restored the transmission of cortical force to cell membrane in spectrin mutant PECs: unlike spectrin mutant PECs that showed apical expansion despite elevated myosin II activity (Fig. 1, E and E'), the *α-spec cpa* double mutant 1° PECs became sensitive to the elevated myosin II activity and showed dramatic apical constriction (Fig. 7, D–D"' and G), even though *cpa* RNAi in wild-type background did not result in obvious apical constriction (Fig. 7, C–C"' and G). This rescue largely depended on myosin II activity, since incubating the mosaic imaginal discs with the Rok inhibitor Y27632 abolished apical constriction in the double mutant cells (Fig. 7, E–E"' and G).

As an important control for this experiment, we compared the effect of increasing F-actin by Myr-WASp overexpression. Unlike the CP-dependent F-actin pool, the F-actin pool resulting from Myr-WASp overexpression interacts with spectrin, as shown above (Fig. 6, A–B'), and likely requires spectrin for attachment to cell membrane. Indeed, Myr-WASp overexpression did not rescue the decreased cortical F-actin in *α-spec* mutant PECs in the presence of Triton X-100 (Fig. S5, A–B); accordingly, the Myr-WASp–overexpressing *α-spec* mutant 1° PECs still showed apical expansion (Fig. S5, E–F"; quantified in Fig. 7 G). Interestingly, overexpressing Myr-WASp in *cpa/α-spec* double RNAi PECs still showed decreased cortical F-actin that resembles Myr-WASp overexpression in α-spec RNAi PECs (Fig. S5, C–D), suggesting that the bulk of F-actin in these cells requires spectrin to be anchored to the cell cortex. These results further corroborate our model that spectrin performs a crucial function by attaching cortical F-actin to cell membrane domains outside of AJs and in turn translates cortical tension into cell shape changes (Fig. 8).

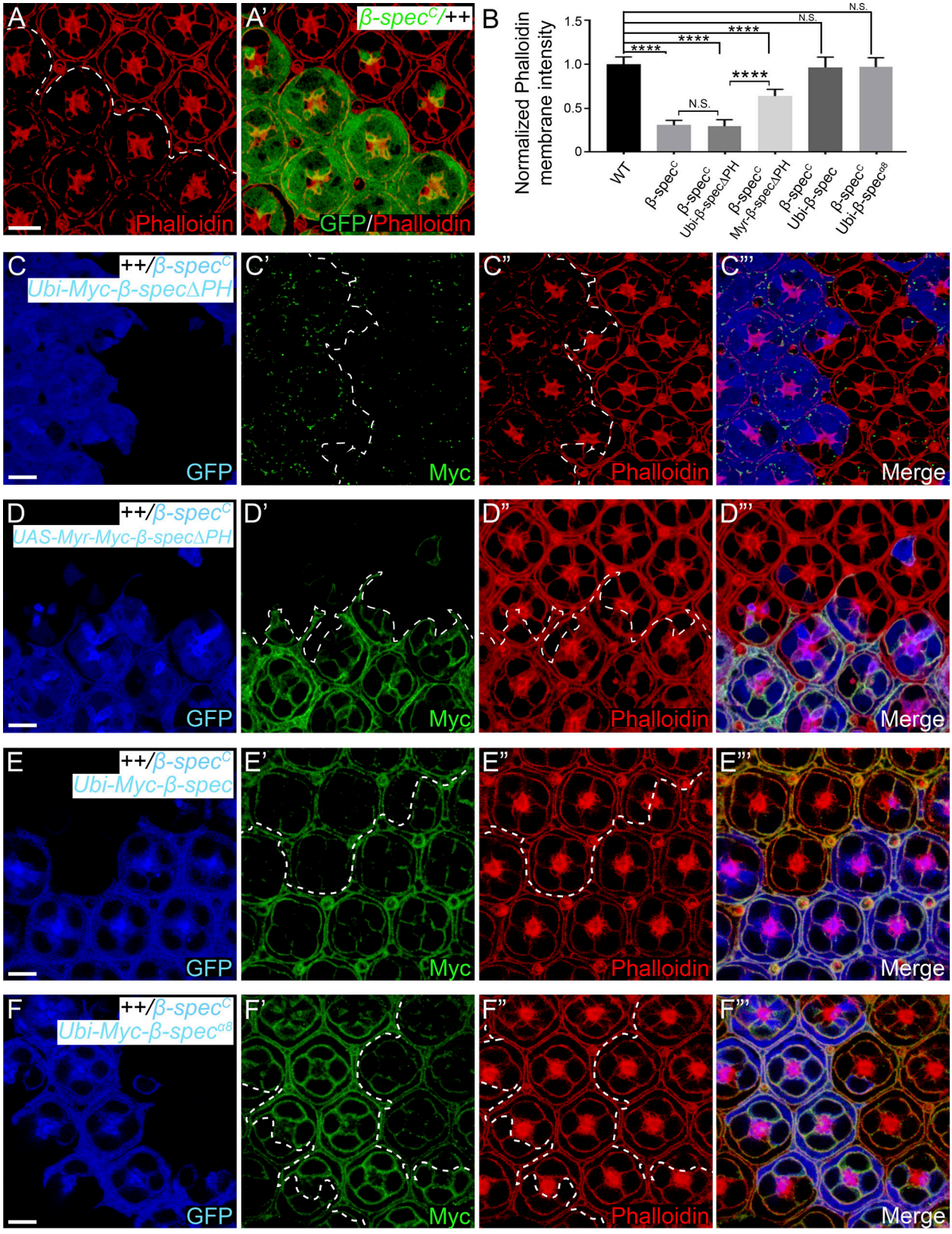

Figure 5. **The association of spectrin with cell membrane requires the PH domain of β-Spec, but not its Ank-binding domain.** All images are z-projections at lateral position. **(A and A')** A Triton X-100–permeabilized pupal eye disc containing GFP-positive *β-spec*^{C} mutant MARCM clones was stained for phalloidin. Note the decreased cortical F-actin level in *β-spec*^{C} mutant PECs. **(B)** Normalized mean phalloidin membrane intensity in A, C", D", E", and F". Data are means ± SEM ($n \geq 20$ cells, representative of five animals). ****, $P < 0.0001$. N.S., no significance. **(C–F'")** Triton X-100–permeabilized pupal eye discs containing GFP-positive MARCM clones of the indicated genotypes were stained for Myc (epitope on the β-Spec transgenes) and phalloidin. Note the failure of

β-SpecΔPH to localize to cell membrane and its inability to rescue cortical F-actin level in *β-spec*^{C} mutant PECs (C–C′″). By contrast, Myr-β-SpecΔPH (D–D′″), wild-type β-Spec (E–E′″), or β-Spec$^{\alpha 8}$ (F–F′″) accumulated on cell membrane and rescued the cortical F-actin level in *β-spec*^{C} mutant PECs. Quantification of phalloidin membrane intensity is shown in B. Scale bars, 5 µm.

Discussion

Although the actomyosin cytoskeleton has been reported to couple cell shape and Yki/YAP activity, the precise mechanisms are poorly understood. Here, we identified spectrin as a critical coupler between cell shape and actomyosin-mediated Yki activation in *Drosophila* retina morphogenesis. We found that the spectrin-mediated SBMS, a cytoskeleton directly underneath the plasma membrane, is an essential part of the mechanotransduction machinery that is responsible for regulating cell shape through transmitting force from the cortical actomyosin to cell membrane domains outside of AJs; however, the transmission of cortex force to membrane domains at AJs is still normal in spectrin mutant PECs, leading to high tension on AJs, which then recruit Jub and Wts, causing Yki activation and overproliferation of cells with abnormal shape (Fig. 8). Therefore, this uncoupling between cell shape and Yki-mediated cell proliferation in spectrin mutant tissue could result in defect in tissue morphogenesis, such as that we observed in spectrin mutant retina (Fig. 1, G and G′).

Although spectrin is known to cross-link with short F-actin to form a latticelike network that supports the structural stability of the plasma membrane in erythrocytes, our study

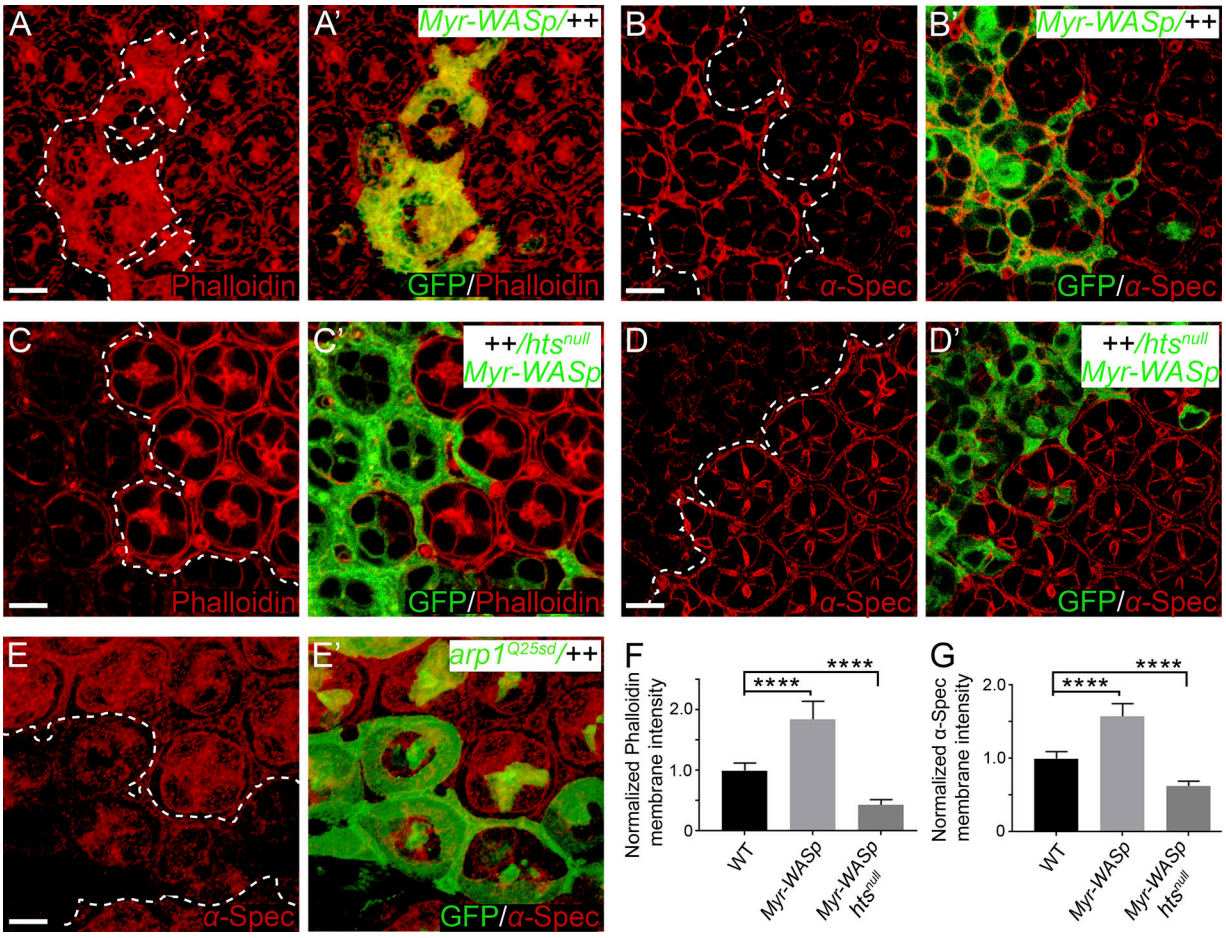

Figure 6. **Myr-WASp promotes the recruitment of α-Spec to the cell cortex.** All images are z-projections at lateral position. **(A and A′)** A Triton X-100–permeabilized pupal eye disc containing GFP-positive MARCM clones with Myr-WASp overexpression was stained for phalloidin. Note the increased cortical F-actin level in the overexpression clones. Quantification of phalloidin membrane intensity is shown in F. **(B and B′)** Similar to A and A′ except that α-Spec staining was examined. Note the increased cortical α-Spec level in the overexpression clones. Quantification of α-Spec membrane intensity is shown in G. **(C and C′)** A Triton X-100–permeabilized pupal eye disc containing GFP-positive *hts*^{null} mutant MARCM clones with Myr-WASp overexpression was stained for phalloidin. Note the decreased cortical F-actin level in *hts*^{null} mutant clones with Myr-WASp overexpression. Quantification of phalloidin membrane intensity is shown in F. **(D and D′)** Similar to C and C′ except that α-Spec staining was examined. Note the decreased cortical α-Spec level in *hts*^{null} mutant clones with Myr-WASp overexpression. Quantification of α-Spec membrane intensity is shown in G. **(E and E′)** A pupal eye disc containing GFP-positive *arpc1*^{Q25sd} mutant MARCM clones was stained for α-Spec. Note the decreased cortical α-Spec level in *arpc1* mutant clones. **(F and G)** Normalized mean membrane intensity of α-Spec or phalloidin staining for the indicated genotypes. Data are means ± SEM ($n \geq 20$ cells, representative of five animals). ****, $P < 0.0001$. Scale bars, 5 µm.

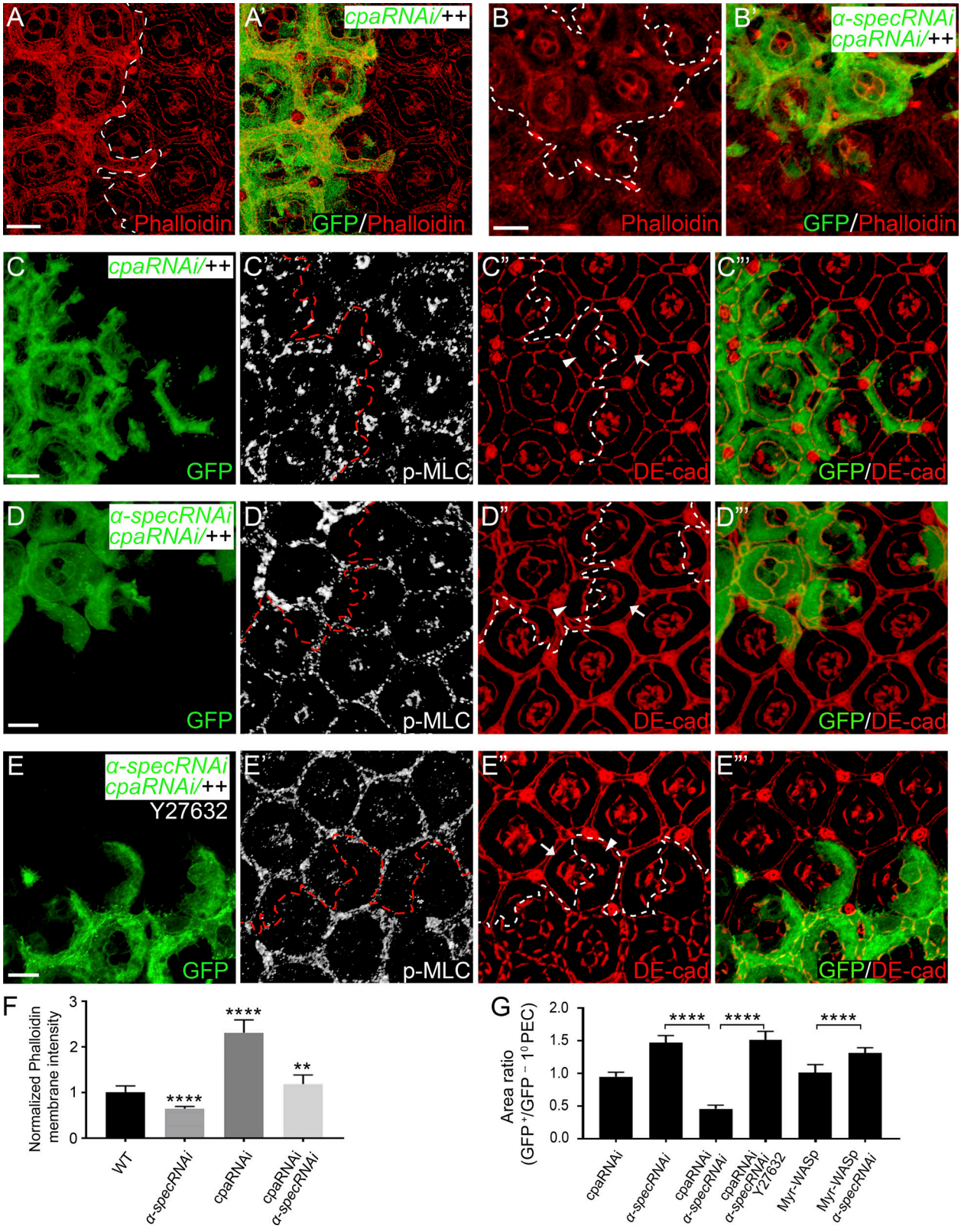

Figure 7. **Cortical F-actin and cell shape defects in spectrin mutant PECs are rescued by inactivation of *cpa*.** The z-projections at apical domain (A and B) and AJs (C–E), respectively. **(A and A')** A Triton X-100–permeabilized pupal eye disc containing GFP-positive MARCM clones with *cpa* RNAi was stained for phalloidin. Note the increased cortical F-actin level in *cpa* mutant PECs. Quantification of phalloidin membrane intensity is shown in F. **(B and B')** Similar to A and A' except that MARCM clones with RNAi of both *cpa* and *α-spec* were examined. Note the modestly increased cortical F-actin level in the mutant PECs. Quantification of phalloidin membrane intensity is shown in F. **(C–C"')** A pupal eye disc containing GFP-positive MARCM clones with *cpa* RNAi was stained for p-MLC (white, C') and DE-cad (red, C"). Note the normal p-MLC level in the mutant PECs. Also note the normal apical area of *cpa* mutant 1° PEC (arrowhead, C")

compared with the wild-type 1° PEC (arrow, C″) in the same mosaic ommatidium. Quantification of apical area of 1° PEC is shown in G. **(D–D‴)** Similar to C–C‴ except that MARCM clones with RNAi of both *cpa* and *α-spec* were examined. Note the increased p-MLC level in the mutant PECs. Also note the dramatic decrease in apical area in the mutant 1° PEC (arrowhead, D″) compared with the wild-type 1° PEC (arrow, D″) in the same mosaic ommatidium. Quantification of apical area of 1° PEC is shown in G. **(E–E‴)** Similar to D–D‴ except that the eye disc was treated by the Rok inhibitor Y27632 for 1 h before fixation. Note the similar p-MLC level inside and outside the mutant clones (E′). Also note the increased apical area in the mutant 1° PEC (arrowhead, E″) compared with the wild-type 1° PEC (arrow, E″) in the same mosaic ommatidium. Quantification of apical area of 1° PEC is shown in G. **(F)** Normalized mean phalloidin membrane intensity analyzed in A–B. Data are means ± SEM ($n \geq 20$ cells, representative of five animals). ****, $P < 0.0001$; **, $P < 0.01$ (Student's *t* test, all compared with wild type). **(G)** Quantification of 1° PECs apical area of the indicated genotypes analyzed in C–E (means ± SEM, $n = 15$ for each genotype). ****, $P < 0.0001$. Scale bars, 5 µm.

uncovers an essential and novel role for spectrin in regulating cell shape by attaching F-actin to cell membrane outside of AJs. Despite normal cortex F-actin level, loss of spectrin function leads to defects in establishing proper intercellular surface tension that in turn compromises proper cell shape and cell organization. The mutual dependence of spectrin and F-actin in membrane association further suggests a feed-forward mechanism for anchoring spectrin-based and the actin-based cytoskeletons to cell membrane. Our study also establishes the *Drosophila* pupal retina as an in vivo model to explore the relationship between mechanical signal and Hippo signaling at single-cell resolution. This in vivo model should complement ongoing studies to dissect mechanosensitive regulation of Hippo signaling using cultured cells.

The prevailing paradigm of how animal cell shape is controlled during tissue morphogenesis suggests that AJs and AJ-associated cortical actomyosin play a key role in dictating cell shape by integrating cell–cell adhesion force and cell cortical tension (Fig. 1 A). However, our results uncover the importance of non–AJ-associated actomyosin in controlling cell shape, since spectrin mutant PECs do not undergo proper cell shape changes in response to enhanced myosin II activity despite normal mechanotransduction machinery at the AJs. Interestingly, actin polymerization promoted by activation of Arp2/3 complex increased the recruitment of spectrin to cell cortex in an adducin-dependent manner. By contrast, actin polymerization promoted by *cpa* RNAi or activation of Dia does not recruit spectrin to cell cortex. Since Arp2/3 catalyzes the initiation of cortical F-actin polymerization while Cpa and Dia regulate the elongation of cortical F-actin, we speculate that spectrin is incorporated into non–AJ-associated actomyosin through adducin after actin polymerization is initiated by the Arp2/3 complex. After this initiation step, the cortical F-actin elongated by Ena or Dia does not incorporate spectrin and these F-actin pools may be attached to cell membrane through spectrin-independent mechanisms. The existence of spectrin-dependent and -independent cortical F-actin pools suggests that changes in the relative amount of different F-actin pools, such as those resulting from activating Arp2/3, may modulate force transmission to cell membrane.

The contraction force of actomyosin cytoskeleton has been shown to regulate cell shape and cell proliferation (Aragona et al., 2013; Rauskolb et al., 2014; Rauzi and Lenne, 2011; Warner and Longmore, 2009a). Does cell shape change itself

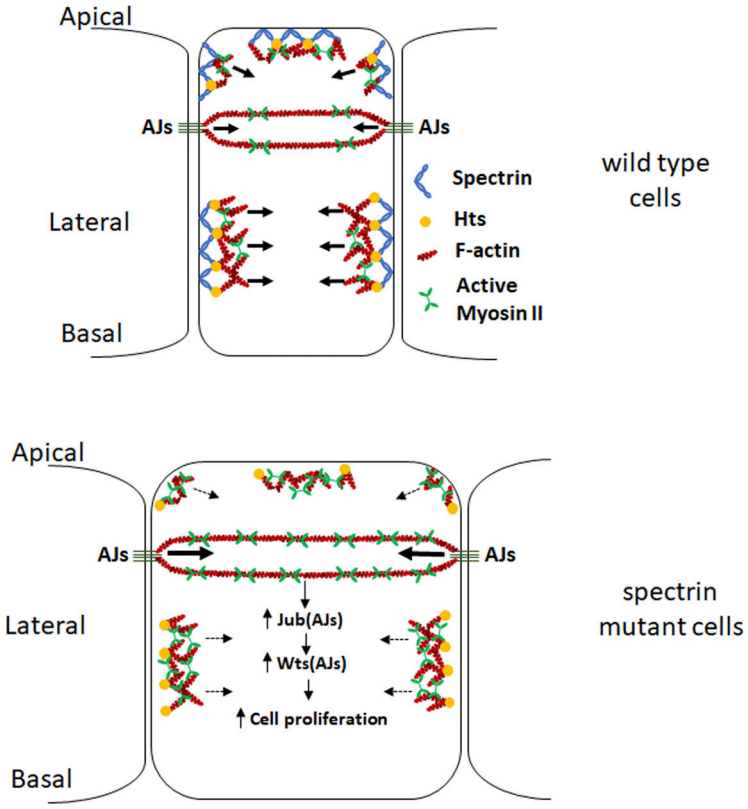

Figure 8. **A schematic model depicting the role of spectrin in coupling cell shape, cortical tension, and Hippo signaling.** Top: WASp-mediated actin polymerization causes Hts-dependent recruitment of spectrin to cellular cortex, where spectrin tethers newly produced F-actin to cell membrane and transmits cortical actomyosin force to cell membrane to support appropriate cell shape. Bottom: Activation of myosin II in spectrin mutant PECs causes higher tension at AJs (larger arrows), leading to accumulation of Jub-Wts complex at AJs and inhibition of Wts activity, which in turn activates Yki and cell proliferation. However, cortical tension at non–AJ membrane domains is lower due to the failure of transmitting cortical actomyosin force to cell membrane (dashed arrows), leading to expanded cell diameter.

regulate cell proliferation? It is possible that cell shape changes can directly stretch cell membrane, which in turn can be sensed by certain stretch-regulated ion channels that regulate the influx of ions such as calcium (Diz-Muñoz et al., 2013; Gudipaty et al., 2017; Pathak et al., 2014). Indeed, cell stretching has been reported to activate the calcium channel Piezo1 to regulate calcium-dependent cell proliferation (Gudipaty et al., 2017). However, since opposite cell shape changes in the same cell type (apical constriction by overexpressing Sqh^{EE} versus apical expansion by loss of spectrin) can both result in Yki-mediated hyperplasia, our study suggests that cell shape per se is not a determinant of Yki activity or cell proliferation. Rather, independent of cell shape, increased actomyosin tension at the AJs would promote Yki activation.

The ability of spectrin in transmitting cortical tension to cell membrane and thus dictating cell shape changes is dependent on its interactions with cortical F-actin and cell membrane. These interactions may be subjected to additional regulation. As we have shown in this study, adducin modulates the association of cortical F-actin with cell membrane in imaginal disc epithelial cells. Interestingly, phosphorylation of adducin by Rok has been reported to promote the interactions between adducin and spectrin (Fukata et al., 1999a, 1999b; Kimura et al., 1998; Tamaru et al., 2005), although we did not observe any changes in the level of cortical spectrin or Hts in cells overexpressing Rok^{CAT} (data not shown). In addition, the PH domain–dependent interactions between spectrin and cell membrane in imaginal disc epithelia suggest that turnover of phosphoinositides (e.g., phosphatidylinositol 4,5-bisphosphate and/or phosphatidylinositol (3,4,5)-trisphosphate) may also regulate the activity of spectrin. This may provide a potential explanation for the genetic requirement of phosphatidylinositol 4-kinase in regulating Yki activity in *Drosophila* (Yan et al., 2011). Taken together, our identification of spectrin as a molecular bridge in transmitting cortical tension to cell membrane not only uncovers an essential mechanism that couples cell shape, cortical tension, and Yki-mediated cell proliferation but also provides a novel entry point to dissect the mechanosensitive regulation of Yki in tissue morphogenesis.

Materials and methods

Drosophila genetics

UAS-α-specRNAi and *UAS-Dank1RNAi* lines were obtained from Vienna Drosophila Resource Center (VDRC; stock IDs 25387, 25945, and 25946). *UAS-rokRNAi*, *UAS-cpaRNAi*, *UAS-dia^{CA}*, and *UAS-DEcad::αCat* lines were obtained from the Bloomington Drosophila Stock Center (stock IDs 34324, 27616, 6669, and 65580). The *tub-GFP-α-spec*, *UAS-mCD8-GFP-utABD*, and *UAS-Myr-Myc-β-specΔPH* fly lines were made in our laboratory, and the Hts-GFP fly line was obtained from VDRC (stock ID 318163). The following flies have been described previously: *α-spec^{rg41}* (Lee et al., 1993); *arpc1^{Q25sd}* (Hudson and Cooley, 2002); *cora^{5}* (Ward et al., 1998); *hts^{null}* (Ohler et al., 2011); *β-spec^{C}* (Yamamoto et al., 2014); *ena^{46}* (Li et al., 2005); *UAS-Myr-WASp* (Bertet et al., 2009); *UAS-Rok^{CAT}* and *UAS-Sqh^{EE}* (Winter et al., 2001); *UAS-DEcad::αCat* (Dumstrei et al., 2002); *UAS-dia^{CA}* (Somogyi and Rørth, 2004); Jub-GFP and Wts-GFP (Rauskolb et al., 2014); *sqh-utABD-GFP* (Rauzi et al., 2010); and *Ubi-Myc-β-spec*, *Ubi-Myc-β-specΔPH*, and *Ubi-Myc-β-spec^{α8}* (Das et al., 2006; Mazock et al., 2010). All crosses were done at 25°C. Genotypes used for clonal analysis are presented below.

Control mosaic analysis with a repressible cell marker (MARCM) clones

UAS-GFP hs-flp; tub-Gal80 FRT40A/FRT40A; tub-Gal4/+.

MARCM clones with RNAi of α-spec, cpa, Dank1, *or* rok

(a) *UAS-GFP hs-flp; tub-Gal80 FRT40A/FRT40A UAS-α-specRNAi; tub-Gal4/+*, (b) *UAS-GFP hs-flp; tub-Gal80 FRT40A/FRT40A; tub-Gal4/UAS-cpaRNAi*, (c) *UAS-GFP hs-flp; tub-Gal80 FRT40A/FRT40A; tub-Gal4/UAS-Dank1RNAi*, and (d) *UAS-GFP hs-flp; tub-Gal80 FRT40A/FRT40A; tub-Gal4/UAS-rokRNAi.*

MARCM clones expressing constitutively active MLC (Sqh^{EE}), Rok^{CAT}, Dia^{CA}, or Myr-WASp

(a) *UAS-GFP hs-flp; tub-Gal80 FRT40A/FRT40A UAS-sqh^{EE}; tub-Gal4/+*, (b) *UAS-GFP hs-flp; tub-Gal80 FRT40A/FRT40A UAS-Rok^{CAT}; tub-Gal4/+*, (c) *UAS-GFP hs-flp; tub-Gal80 FRT40A/FRT40A; tub-Gal4/UAS-dia^{CA}*, and (d) *UAS-GFP hs-flp; tub-Gal80 FRT40A/FRT40A UAS-Myr-WASp; tub-Gal4/+.*

hts^{null} *mutant MARCM clones with overexpression of Myr-WASp*

UAS-GFP hs-flp; tub-Gal80 FRT42D/FRT42D hts^{null} UAS-Myr-WASp; tub-Gal4/+.

MARCM clones with α-spec *RNAi and RNAi of* rok *or* cpa

UAS-GFP hs-flp; tub-Gal80 FRT40A/FRT40A UAS-α-specRNAi; tub-Gal4/UAS-rokRNAi and *UAS-GFP hs-flp; tub-Gal80 FRT40A/FRT40A UAS-α-specRNAi; tub-Gal4/UAS-cpaRNAi.*

MARCM clones with α-spec *RNAi and overexpression of Sqh^{EE}, Rok^{CAT}, mCD8-GFP-utABD, Myr-WASp, or DEcad::αCat*

(a) *UAS-GFP hs-flp; tub-Gal80 FRT40A/FRT40A UAS-α-specRNAi, UAS-sqh^{EE}; tub-Gal4/+*, (b) *UAS-GFP hs-flp; tub-Gal80 FRT40A/FRT40A UAS-α-specRNAi, UAS-Rok^{CAT}; tub-Gal4/+*, (c) *UAS-GFP hs-flp; tub-Gal80 FRT40A/FRT40A UAS-α-specRNAi; tub-Gal4/UAS-mCD8-GFP-utABD*, (d) *UAS-GFP hs-flp; tub-Gal80 FRT40A/FRT40A UAS-α-specRNAi, UAS-Myr-WASp; tub-Gal4/+*, (e) *UAS-GFP hs-flp; tub-Gal80 FRT40A/FRT40A UAS-α-specRNAi, UAS-Myr-WASp; tub-Gal4/UAS-cpaRNAi*, and (f) *UAS-GFP hs-flp; tub-Gal80 FRT40A/FRT40A UAS-α-specRNAi; tub-Gal4/UAS-DEcad::αCat.*

α-spec^{rg41}, hts^{null}, cora^{5}, ena^{46}, or β-spec^{C} mutant clones

(a) *hs-flp; Ubi-GFP FRT80B/FRT80B α-spec^{rg41}*, (b) *hs-flp; Ubi-GFP FRT42D/FRT42D hts^{null}*, (c) *UAS-GFP hs-flp; tub-Gal80 FRT42D/FRT42D hts^{null}; tub-Gal4/+*, (d) *hs-flp; Ubi-GFP FRT42D/FRT42D cora^{5}*, (e) *UAS-GFP hs-flp; tub-Gal80 FRT42D/FRT42D ena^{46}; tub-Gal4/+*, and (f) *19A β-spec^{C}/19A tub-Gal80 hs-flp; UAS-GFP/+; tub-Gal4/+.*

β-spec^{C} *mutant MARCM clones with overexpression of Myc-β-spec, Myc-β-specΔPH, Myr-Myc-β-specΔPH, or Myc-β-spec^{α8}*

(a) *19A β-spec^{C}/19A tub-Gal80 hs-flp; UAS-GFP/+; tub-Gal4/Ubi-Myc-β-spec*, (b) *19A β-spec^{C}/19A tub-Gal80 hs-flp; UAS-GFP/+;*

tub-Gal4/Ubi-Myc-β-specΔPH, (c) *19A β-spec^{C}/19A tub-Gal80 hs-flp; UAS-GFP/UAS-Myr-Myc-β-specΔPH; tub-Gal4/+*, and (d) *19A β-spec^{C}, Ubi-Myc-β-spec$^{\alpha 8}$/19A tub-Gal80 hs-flp; UAS-GFP/+; tub-Gal4/+*.

Immunofluorescence

Pupal eyes or wing imaginal discs were fixed and stained following standard formaldehyde fixation and permeabilization/washes in PBS containing 0.3% Triton X-100. All pupal eyes were fixed ∼40 h APF unless otherwise specified. For phalloidin staining after Triton X-100 permeabilization, tissue was fixed first, incubated in PBS containing 0.3% Triton X-100 and 5% goat serum for 1 h, and then washed three times in PBS with 5% goat serum and stained with phalloidin in PBS with 5% goat serum for 30 min. The following antibodies were used: rat anti–DE-cad (1:10), mouse anti–α-Spec (1:50), mouse anti-Dlg (1:50), mouse anti-Ena (1:50; all from the Developmental Studies Hybridoma Bank), mouse anti-Myc (1:200, clone 9E10; Millipore Sigma), rabbit anti-pMLC (1:10; Cell Signaling Technologies), rabbit anti–PAR-3 (1:1,000; provided by A. Wodarz, Univesity of Cologne, Cologne, Germany; Wodarz et al., 1999). Alexa Fluor 568 phalloidin (1:50; Invitrogen) was used to visualize F-actin.

In experiments involving treatment of Rok inhibitor, pupal eyes were incubated with 1 mM Y27632 in Schneider's *Drosophila* medium (GIBCO BRL, Life Technologies) for 1 h before fixation as described previously (Legoff et al., 2013).

Microscope image acquisition

All imaging was performed at room temperature through a Zeiss LSM 880 Axio observer confocal microscope with Airyscan using a 40× objective. The 40× objective for the LSM 880 confocal microscope was a Plan-apochromat oil-immersion objective for Airyscan with a numerical aperture of 1.3. Fluorescent donkey or goat secondary antibodies were used that were conjugated to Alexa Fluor 568, Cy3, Cy5, or Alexa Fluor 647. All specimens were mounted in VECTASHIELD antifade mounting media (Vector Laboratories) before imaging. Zen 2.1 software was used to acquire and export all images as LSM files. ImageJ (version 1.52a) was used to open and analyze images. Adobe Photoshop and Illustrator were used to make figures. Unless otherwise indicated, all images shown in the figures represent z-projections of multiple optic sections at the specified position along the apical-basal axis.

Image quantification

Intensity measurement. Lateral membrane or junctional intensity measurements were performed on maximum projections of corresponding cell area (2 µm) using the freehand line tool (with a width line of six pixels) in ImageJ (version 1.52a) after a single background subtraction (rolling ball radius, 200 pixels). Apical membrane intensity measurements were performed on maximum projections of cell apical area (3 µm) using the freehand selection tool in ImageJ to draw the cell contour and then measure the mean intensity, after a single background subtraction (rolling ball radius, 200 pixels). For comparing intensity values in pupal eye discs of different genetic background, intensity from cells of a genetic background was normalized to the mean from the wild-type cells of the same pupal eye disc.

Area measurement

Cell area measurements were performed using the freehand selections tool in ImageJ to draw the cell contour and measure the area. For comparing ommatidium area values in pupal eye discs of different genetic background, area of an ommatidium constituted fully of a specific genotype was normalized to the mean of fully wild-type ommatidia from the same pupal eye disc.

MPA

Drosophila imaginal wing discs were dissected from third instar larvae and digested into single cells for MPA according to procedures described previously (Khan et al., 2016). Capillary glass (A-M Systems, Inc.) was pulled using a P-1000 micropipette puller (Sutter Instrument). The diameter of pipette tip ranged from 5.2 to 7.8 µm. Cell diameter ranged from 8.2 to 14.7 µm. Ratio of the diameter of pipette tip to that of a cell during micro-aspiration was 0.61 ± 0.03 (mean ± SEM, n ≥ 15). The tip of the pipette was polished and bended for 20° using microforge MF-830 (Narishige International USA, Inc.). The pipette was filled with 1× PBS without calcium and magnesium (Mediatech, Inc.) that was supplemented with 10% FBS (certified, U.S. origin, GIBCO BRL, Thermo Fisher Scientific), and mounted to a micromanipulator (Leica) for micro-aspiration under a microscope (Elipse TE 2000-u; Nikon). The angle of the pipette on micromanipulator was adjusted to make the pipette tip in a horizontal plane. The pipette holder has a side outlet connected to a high-speed pressure clamp (ALA Scientific Instruments) for application of pressure in a timely manner, with which pressure of −200 to 200 mmHg could be applied with a small increment of 0.1 mmHg. Before micro-aspiration, zeroing of the instrument was done and confirmed by observing no movement of a small debris inside the pipette tip. Images of cells during micro-aspiration were taken by a digital still camera for microscope DXM 1200 (Nikon) under differential interference contrast mode, and corresponding pressure applied was recorded at the same time. The pressure (ΔP) with which cell length aspirated into pipette equals the radius of pipette tip (Rp) was used for cortical tension calculation with a Laplace law equation, $\Delta P = 2Teff\left(\frac{1}{Rp} - \frac{1}{Rc}\right)$, where Teff is effective cortical tension and Rc is the radius of cell at ΔP (Hochmuth, 2000; Luo et al., 2013; Rauzi and Lenne, 2011; Sun et al., 2014).

Online supplemental material

Fig. S1 shows further analysis of the coupling between cell shape and myosin II activity in wild-type and spectrin mutant PECs. Fig. S2 shows analysis of ommatidia size, cell polarity, and Ena expression/function in pupal retina. Fig. S3 shows analysis of cortical F-actin and cell shape in *hts^{null}* mutant PECs. Fig. S4 shows analysis of cortical α-Spec level in different genetic background and the importance of the PH domain of β-Spec in cell shape determination. Fig. S5 shows that Myr-WASp overexpression did not rescue the cortical F-actin and cell shape defects in spectrin mutant PECs.

Acknowledgments

We thank A. Wodarz for providing PAR-3 antibody. We also thank T. Lecuit, T. Suzuki, R. Dubreuil, the Bloomington and

Vienna Stock Centers, and the Developmental Studies Hybridoma Bank for reagents. This work was supported in part by grants from the National Institutes of Health (EY015708 to D. Pan and GM121780 to P. Blount) and the Welch Foundation (I-1420 to P. Blount). D. Pan is an investigator of the Howard Hughes Medical Institute.

The authors declare no competing financial interests.

Author contributions: H. Deng and D. Pan conceived the study, designed experiments, interpreted data, and wrote the article. L. Yang and P. Blount performed and analyzed the micropipette aspiration experiment. P. Wen and H. Lei designed and made DNA constructs for the transgenic flies.

Submitted: 3 July 2019
Revised: 26 November 2019
Accepted: 17 January 2020

References

Aragona, M., T. Panciera, A. Manfrin, S. Giulitti, F. Michielin, N. Elvassore, S. Dupont, and S. Piccolo. 2013. A mechanical checkpoint controls multicellular growth through YAP/TAZ regulation by actin-processing factors. *Cell.* 154:1047–1059. https://doi.org/10.1016/j.cell.2013.07.042

Bennett, V., and A.J. Baines. 2001. Spectrin and ankyrin-based pathways: metazoan inventions for integrating cells into tissues. *Physiol. Rev.* 81: 1353–1392. https://doi.org/10.1152/physrev.2001.81.3.1353

Bennett, V., K. Gardner, and J.P. Steiner. 1988. Brain adducin: a protein kinase C substrate that may mediate site-directed assembly at the spectrin-actin junction. *J. Biol. Chem.* 263:5860–5869.

Benz, P.M., C. Blume, J. Moebius, C. Oschatz, K. Schuh, A. Sickmann, U. Walter, S.M. Feller, and T. Renné. 2008. Cytoskeleton assembly at endothelial cell-cell contacts is regulated by alphaII-spectrin-VASP complexes. *J. Cell Biol.* 180:205–219. https://doi.org/10.1083/jcb.200709181

Benz, P.M., C.J. Merkel, K. Offner, M. Abeßer, M. Ullrich, T. Fischer, B. Bayer, H. Wagner, S. Gambaryan, J.A. Ursitti, et al. 2013. Mena/VASP and αII-Spectrin complexes regulate cytoplasmic actin networks in cardiomyocytes and protect from conduction abnormalities and dilated cardiomyopathy. *Cell Commun. Signal.* 11:56. https://doi.org/10.1186/1478-811X-11-56

Bertet, C., M. Rauzi, and T. Lecuit. 2009. Repression of Wasp by JAK/STAT signalling inhibits medial actomyosin network assembly and apical cell constriction in intercalating epithelial cells. *Development.* 136:4199–4212. https://doi.org/10.1242/dev.040402

Burkel, B.M., G. von Dassow, and W.M. Bement. 2007. Versatile fluorescent probes for actin filaments based on the actin-binding domain of utrophin. *Cell Motil. Cytoskeleton.* 64:822–832. https://doi.org/10.1002/cm.20226

Butcher, D.T., T. Alliston, and V.M. Weaver. 2009. A tense situation: forcing tumour progression. *Nat. Rev. Cancer.* 9:108–122. https://doi.org/10.1038/nrc2544

Cagan, R.L., and D.F. Ready. 1989. The emergence of order in the Drosophila pupal retina. *Dev. Biol.* 136:346–362. https://doi.org/10.1016/0012-1606(89)90261-3

Campellone, K.G., and M.D. Welch. 2010. A nucleator arms race: cellular control of actin assembly. *Nat. Rev. Mol. Cell Biol.* 11:237–251. https://doi.org/10.1038/nrm2867

Carthew, R.W. 2007. Pattern formation in the Drosophila eye. *Curr. Opin. Genet. Dev.* 17:309–313. https://doi.org/10.1016/j.gde.2007.05.001

Coravos, J.S., and A.C. Martin. 2016. Apical sarcomere-like actomyosin contracts nonmuscle Drosophila epithelial cells. *Dev. Cell.* 39:346–358. https://doi.org/10.1016/j.devcel.2016.09.023

Das, A., C. Base, S. Dhulipala, and R.R. Dubreuil. 2006. Spectrin functions upstream of ankyrin in a spectrin cytoskeleton assembly pathway. *J. Cell Biol.* 175:325–335. https://doi.org/10.1083/jcb.200602095

Deng, H., W. Wang, J. Yu, Y. Zheng, Y. Qing, and D. Pan. 2015. Spectrin regulates Hippo signaling by modulating cortical actomyosin activity. *eLife.* 4:e06567. https://doi.org/10.7554/eLife.06567

Discher, D.E., D.J. Mooney, and P.W. Zandstra. 2009. Growth factors, matrices, and forces combine and control stem cells. *Science.* 324:1673–1677. https://doi.org/10.1126/science.1171643

Diz-Muñoz, A., D.A. Fletcher, and O.D. Weiner. 2013. Use the force: membrane tension as an organizer of cell shape and motility. *Trends Cell Biol.* 23:47–53. https://doi.org/10.1016/j.tcb.2012.09.006

Doherty, G.J., and H.T. McMahon. 2008. Mediation, modulation, and consequences of membrane-cytoskeleton interactions. *Annu. Rev. Biophys.* 37:65–95. https://doi.org/10.1146/annurev.biophys.37.032807.125912

Dumstrei, K., F. Wang, D. Shy, U. Tepass, and V. Hartenstein. 2002. Interaction between EGFR signaling and DE-cadherin during nervous system morphogenesis. *Development.* 129:3983–3994.

Dupont, S., L. Morsut, M. Aragona, E. Enzo, S. Giulitti, M. Cordenonsi, F. Zanconato, J. Le Digabel, M. Forcato, S. Bicciato, et al. 2011. Role of YAP/TAZ in mechanotransduction. *Nature.* 474:179–183. https://doi.org/10.1038/nature10137

Edwards, M., A. Zwolak, D.A. Schafer, D. Sept, R. Dominguez, and J.A. Cooper. 2014. Capping protein regulators fine-tune actin assembly dynamics. *Nat. Rev. Mol. Cell Biol.* 15:677–689. https://doi.org/10.1038/nrm3869

Farge, E. 2011. Mechanotransduction in development. *Curr. Top. Dev. Biol.* 95: 243–265. https://doi.org/10.1016/B978-0-12-385065-2.00008-6

Fernández, B.G., P. Gaspar, C. Brás-Pereira, B. Jezowska, S.R. Rebelo, and F. Janody. 2011. Actin-Capping Protein and the Hippo pathway regulate F-actin and tissue growth in Drosophila. *Development.* 138:2337–2346. https://doi.org/10.1242/dev.063545

Fletcher, G.C., A. Elbediwy, I. Khanal, P.S. Ribeiro, N. Tapon, and B.J. Thompson. 2015. The Spectrin cytoskeleton regulates the Hippo signalling pathway. *EMBO J.* 34:940–954. https://doi.org/10.15252/embj.201489642

Folkman, J., and A. Moscona. 1978. Role of cell shape in growth control. *Nature.* 273:345–349. https://doi.org/10.1038/273345a0

Fukata, Y., N. Oshiro, and K. Kaibuchi. 1999a. Activation of moesin and adducin by Rho-kinase downstream of Rho. *Biophys. Chem.* 82:139–147. https://doi.org/10.1016/S0301-4622(99)00113-1

Fukata, Y., N. Oshiro, N. Kinoshita, Y. Kawano, Y. Matsuoka, V. Bennett, Y. Matsuura, and K. Kaibuchi. 1999b. Phosphorylation of adducin by Rho-kinase plays a crucial role in cell motility. *J. Cell Biol.* 145:347–361. https://doi.org/10.1083/jcb.145.2.347

Gardner, K., and V. Bennett. 1987. Modulation of spectrin-actin assembly by erythrocyte adducin. *Nature.* 328:359–362. https://doi.org/10.1038/328359a0

Goley, E.D., and M.D. Welch. 2006. The ARP2/3 complex: an actin nucleator comes of age. *Nat. Rev. Mol. Cell Biol.* 7:713–726. https://doi.org/10.1038/nrm2026

Gudipaty, S.A., J. Lindblom, P.D. Loftus, M.J. Redd, K. Edes, C.F. Davey, V. Krishnegowda, and J. Rosenblatt. 2017. Mechanical stretch triggers rapid epithelial cell division through Piezo1. *Nature.* 543:118–121. https://doi.org/10.1038/nature21407

Halder, G., S. Dupont, and S. Piccolo. 2012. Transduction of mechanical and cytoskeletal cues by YAP and TAZ. *Nat. Rev. Mol. Cell Biol.* 13:591–600. https://doi.org/10.1038/nrm3416

Hamaratoglu, F., M. Willecke, M. Kango-Singh, R. Nolo, E. Hyun, C. Tao, H. Jafar-Nejad, and G. Halder. 2006. The tumour-suppressor genes NF2/Merlin and Expanded act through Hippo signalling to regulate cell proliferation and apoptosis. *Nat. Cell Biol.* 8:27–36. https://doi.org/10.1038/ncb1339

Harris, T.J., and U. Tepass. 2010. Adherens junctions: from molecules to morphogenesis. *Nat. Rev. Mol. Cell Biol.* 11:502–514. https://doi.org/10.1038/nrm2927

Heisenberg, C.P., and Y. Bellaïche. 2013. Forces in tissue morphogenesis and patterning. *Cell.* 153:948–962. https://doi.org/10.1016/j.cell.2013.05.008

Hochmuth, R.M. 2000. Micropipette aspiration of living cells. *J. Biomech.* 33: 15–22. https://doi.org/10.1016/S0021-9290(99)00175-X

Hoffman, B.D., C. Grashoff, and M.A. Schwartz. 2011. Dynamic molecular processes mediate cellular mechanotransduction. *Nature.* 475:316–323. https://doi.org/10.1038/nature10316

Huang, S., and D.E. Ingber. 1999. The structural and mechanical complexity of cell-growth control. *Nat. Cell Biol.* 1:E131–E138. https://doi.org/10.1038/13043

Hudson, A.M., and L. Cooley. 2002. A subset of dynamic actin rearrangements in Drosophila requires the Arp2/3 complex. *J. Cell Biol.* 156: 677–687. https://doi.org/10.1083/jcb.200109065

Kapus, A., and P. Janmey. 2013. Plasma membrane--cortical cytoskeleton interactions: a cell biology approach with biophysical considerations. *Compr. Physiol.* 3:1231–1281.

Kee, Y.S., and D.N. Robinson. 2013. Micropipette aspiration for studying cellular mechanosensory responses and mechanics. *Methods Mol. Biol.* 983:367–382. https://doi.org/10.1007/978-1-62703-302-2_20

Khan, S.J., S.N. Abidi, Y. Tian, A. Skinner, and R.K. Smith-Bolton. 2016. A rapid, gentle and scalable method for dissociation and fluorescent sorting of imaginal disc cells for mRNA sequencing. *Fly (Austin)*. 10: 73–80. https://doi.org/10.1080/19336934.2016.1173296

Kimura, K., Y. Fukata, Y. Matsuoka, V. Bennett, Y. Matsuura, K. Okawa, A. Iwamatsu, and K. Kaibuchi. 1998. Regulation of the association of adducin with actin filaments by Rho-associated kinase (Rho-kinase) and myosin phosphatase. *J. Biol. Chem.* 273:5542–5548. https://doi.org/10.1074/jbc.273.10.5542

Krause, M., E.W. Dent, J.E. Bear, J.J. Loureiro, and F.B. Gertler. 2003. Ena/VASP proteins: regulators of the actin cytoskeleton and cell migration. *Annu. Rev. Cell Dev. Biol.* 19:541–564. https://doi.org/10.1146/annurev.cellbio.19.050103.103356

Lecuit, T., and P.F. Lenne. 2007. Cell surface mechanics and the control of cell shape, tissue patterns and morphogenesis. *Nat. Rev. Mol. Cell Biol.* 8: 633–644. https://doi.org/10.1038/nrm2222

Lecuit, T., P.F. Lenne, and E. Munro. 2011. Force generation, transmission, and integration during cell and tissue morphogenesis. *Annu. Rev. Cell Dev. Biol.* 27:157–184. https://doi.org/10.1146/annurev-cellbio-100109-104027

Lecuit, T., and A.S. Yap. 2015. E-cadherin junctions as active mechanical integrators in tissue dynamics. *Nat. Cell Biol.* 17:533–539. https://doi.org/10.1038/ncb3136

Lee, J.K., E. Brandin, D. Branton, and L.S. Goldstein. 1997. alpha-Spectrin is required for ovarian follicle monolayer integrity in *Drosophila melanogaster*. *Development*. 124:353–362.

Lee, J.K., R.S. Coyne, R.R. Dubreuil, L.S. Goldstein, and D. Branton. 1993. Cell shape and interaction defects in alpha-spectrin mutants of *Drosophila melanogaster*. *J. Cell Biol.* 123:1797–1809. https://doi.org/10.1083/jcb.123.6.1797

Legoff, L., H. Rouault, and T. Lecuit. 2013. A global pattern of mechanical stress polarizes cell divisions and cell shape in the growing Drosophila wing disc. *Development*. 140:4051–4059. https://doi.org/10.1242/dev.090878

Lemmon, M.A. 2008. Membrane recognition by phospholipid-binding domains. *Nat. Rev. Mol. Cell Biol.* 9:99–111. https://doi.org/10.1038/nrm2328

Li, W., Y. Li, and F.B. Gao. 2005. Abelson, enabled, and p120 catenin exert distinct effects on dendritic morphogenesis in Drosophila. *Dev. Dyn.* 234:512–522. https://doi.org/10.1002/dvdy.20496

Li, X., Y. Matsuoka, and V. Bennett. 1998. Adducin preferentially recruits spectrin to the fast growing ends of actin filaments in a complex requiring the MARCKS-related domain and a newly defined oligomerization domain. *J. Biol. Chem.* 273:19329–19338. https://doi.org/10.1074/jbc.273.30.19329

Luo, T., K. Mohan, P.A. Iglesias, and D.N. Robinson. 2013. Molecular mechanisms of cellular mechanosensing. *Nat. Mater.* 12:1064–1071. https://doi.org/10.1038/nmat3772

Machnicka, B., R. Grochowalska, D.M. Bogusławska, A.F. Sikorski, and M.C. Lecomte. 2012. Spectrin-based skeleton as an actor in cell signaling. *Cell. Mol. Life Sci.* 69:191–201. https://doi.org/10.1007/s00018-011-0804-5

Martin, A.C., M. Kaschube, and E.F. Wieschaus. 2009. Pulsed contractions of an actin-myosin network drive apical constriction. *Nature*. 457: 495–499. https://doi.org/10.1038/nature07522

Mazock, G.H., A. Das, C. Base, and R.R. Dubreuil. 2010. Transgene rescue identifies an essential function for Drosophila beta spectrin in the nervous system and a selective requirement for ankyrin-2-binding activity. *Mol. Biol. Cell.* 21:2860–2868. https://doi.org/10.1091/mbc.e10-03-0180

McBeath, R., D.M. Pirone, C.M. Nelson, K. Bhadriraju, and C.S. Chen. 2004. Cell shape, cytoskeletal tension, and RhoA regulate stem cell lineage commitment. *Dev. Cell*. 6:483–495. https://doi.org/10.1016/S1534-5807(04)00075-9

Nelson, C.M., and M.J. Bissell. 2006. Of extracellular matrix, scaffolds, and signaling: tissue architecture regulates development, homeostasis, and cancer. *Annu. Rev. Cell Dev. Biol.* 22:287–309. https://doi.org/10.1146/annurev.cellbio.22.010305.104315

Nelson, C.M., R.P. Jean, J.L. Tan, W.F. Liu, N.J. Sniadecki, A.A. Spector, and C.S. Chen. 2005. Emergent patterns of growth controlled by multicellular form and mechanics. *Proc. Natl. Acad. Sci. USA*. 102:11594–11599. https://doi.org/10.1073/pnas.0502575102

Ohler, S., S. Hakeda-Suzuki, and T. Suzuki. 2011. Hts, the Drosophila homologue of Adducin, physically interacts with the transmembrane receptor Golden goal to guide photoreceptor axons. *Dev. Dyn.* 240:135–148. https://doi.org/10.1002/dvdy.22515

Pathak, M.M., J.L. Nourse, T. Tran, J. Hwe, J. Arulmoli, D.T. Le, E. Bernardis, L.A. Flanagan, and F. Tombola. 2014. Stretch-activated ion channel Piezo1 directs lineage choice in human neural stem cells. *Proc. Natl. Acad. Sci. USA*. 111:16148–16153. https://doi.org/10.1073/pnas.1409802111

Pinder, J.C., and A.J. Baines. 2000. A protein accumulator. *Nature*. 406: 253–254. https://doi.org/10.1038/35018679

Pollard, T.D. 2007. Regulation of actin filament assembly by Arp2/3 complex and formins. *Annu. Rev. Biophys. Biomol. Struct.* 36:451–477. https://doi.org/10.1146/annurev.biophys.35.040405.101936

Pollard, T.D., and G.G. Borisy. 2003. Cellular motility driven by assembly and disassembly of actin filaments. *Cell*. 112:453–465. https://doi.org/10.1016/S0092-8674(03)00120-X

Priya, R., and A.S. Yap. 2015. Active tension: the role of cadherin adhesion and signaling in generating junctional contractility. *Curr. Top. Dev. Biol.* 112:65–102. https://doi.org/10.1016/bs.ctdb.2014.11.016

Puliafito, A., L. Hufnagel, P. Neveu, S. Streichan, A. Sigal, D.K. Fygenson, and B.I. Shraiman. 2012. Collective and single cell behavior in epithelial contact inhibition. *Proc. Natl. Acad. Sci. USA*. 109:739–744. https://doi.org/10.1073/pnas.1007809109

Ratheesh, A., and A.S. Yap. 2012. A bigger picture: classical cadherins and the dynamic actin cytoskeleton. *Nat. Rev. Mol. Cell Biol.* 13:673–679. https://doi.org/10.1038/nrm3431

Rauskolb, C., S. Sun, G. Sun, Y. Pan, and K.D. Irvine. 2014. Cytoskeletal tension inhibits Hippo signaling through an Ajuba-Warts complex. *Cell*. 158:143–156. https://doi.org/10.1016/j.cell.2014.05.035

Rauzi, M., and P.F. Lenne. 2011. Cortical forces in cell shape changes and tissue morphogenesis. *Curr. Top. Dev. Biol.* 95:93–144. https://doi.org/10.1016/B978-0-12-385065-2.00004-9

Rauzi, M., P.F. Lenne, and T. Lecuit. 2010. Planar polarized actomyosin contractile flows control epithelial junction remodelling. *Nature*. 468: 1110–1114. https://doi.org/10.1038/nature09566

Sansores-Garcia, L., W. Bossuyt, K. Wada, S. Yonemura, C. Tao, H. Sasaki, and G. Halder. 2011. Modulating F-actin organization induces organ growth by affecting the Hippo pathway. *EMBO J.* 30:2325–2335. https://doi.org/10.1038/emboj.2011.157

Somlyo, A.P., and A.V. Somlyo. 2003. Ca2+ sensitivity of smooth muscle and nonmuscle myosin II: modulated by G proteins, kinases, and myosin phosphatase. *Physiol. Rev.* 83:1325–1358. https://doi.org/10.1152/physrev.00023.2003

Somogyi, K., and P. Rørth. 2004. Evidence for tension-based regulation of Drosophila MAL and SRF during invasive cell migration. *Dev. Cell*. 7: 85–93. https://doi.org/10.1016/j.devcel.2004.05.020

Spiegelman, B.M., and C.A. Ginty. 1983. Fibronectin modulation of cell shape and lipogenic gene expression in 3T3-adipocytes. *Cell*. 35:657–666. https://doi.org/10.1016/0092-8674(83)90098-3

Sun, Q., T. Luo, Y. Ren, O. Florey, S. Shirasawa, T. Sasazuki, D.N. Robinson, and M. Overholtzer. 2014. Competition between human cells by entosis. *Cell Res.* 24:1299–1310. https://doi.org/10.1038/cr.2014.138

Takenawa, T., and S. Suetsugu. 2007. The WASP-WAVE protein network: connecting the membrane to the cytoskeleton. *Nat. Rev. Mol. Cell Biol.* 8: 37–48. https://doi.org/10.1038/nrm2069

Tamaru, S., T. Fukuta, K. Kaibuchi, Y. Matsuoka, H. Shiku, and M. Nishikawa. 2005. Rho-kinase induces association of adducin with the cytoskeleton in platelet activation. *Biochem. Biophys. Res. Commun.* 332: 347–351. https://doi.org/10.1016/j.bbrc.2005.04.127

Vicente-Manzanares, M., X. Ma, R.S. Adelstein, and A.R. Horwitz. 2009. Nonmuscle myosin II takes centre stage in cell adhesion and migration. *Nat. Rev. Mol. Cell Biol.* 10:778–790. https://doi.org/10.1038/nrm2786

Wada, K., K. Itoga, T. Okano, S. Yonemura, and H. Sasaki. 2011. Hippo pathway regulation by cell morphology and stress fibers. *Development*. 138:3907–3914. https://doi.org/10.1242/dev.070987

Ward, R.E. IV, R.S. Lamb, and R.G. Fehon. 1998. A conserved functional domain of Drosophila coracle is required for localization at the septate junction and has membrane-organizing activity. *J. Cell Biol.* 140: 1463–1473. https://doi.org/10.1083/jcb.140.6.1463

Warner, S.J., and G.D. Longmore. 2009a. Cdc42 antagonizes Rho1 activity at adherens junctions to limit epithelial cell apical tension. *J. Cell Biol.* 187: 119–133. https://doi.org/10.1083/jcb.200906047

Warner, S.J., and G.D. Longmore. 2009b. Distinct functions for Rho1 in maintaining adherens junctions and apical tension in remodeling epithelia. *J. Cell Biol.* 185:1111–1125. https://doi.org/10.1083/jcb.200901029

Winter, C.G., B. Wang, A. Ballew, A. Royou, R. Karess, J.D. Axelrod, and L. Luo. 2001. Drosophila Rho-associated kinase (Drok) links Frizzled-mediated planar cell polarity signaling to the actin cytoskeleton. *Cell*. 105:81–91. https://doi.org/10.1016/S0092-8674(01)00298-7

Wittelsberger, S.C., K. Kleene, and S. Penman. 1981. Progressive loss of shape-responsive metabolic controls in cells with increasingly transformed phenotype. *Cell.* 24:859–866. https://doi.org/10.1016/0092-8674(81)90111-2

Wodarz, A., A. Ramrath, U. Kuchinke, and E. Knust. 1999. Bazooka provides an apical cue for Inscuteable localization in Drosophila neuroblasts. *Nature.* 402:544–547. https://doi.org/10.1038/990128

Wong, K.K., W. Li, Y. An, Y. Duan, Z. Li, Y. Kang, and Y. Yan. 2015. β-Spectrin regulates the hippo signaling pathway and modulates the basal actin network. *J. Biol. Chem.* 290:6397–6407. https://doi.org/10.1074/jbc.M114.629493

Wozniak, M.A., and C.S. Chen. 2009. Mechanotransduction in development: a growing role for contractility. *Nat. Rev. Mol. Cell Biol.* 10:34–43. https://doi.org/10.1038/nrm2592

Yamamoto, S., M. Jaiswal, W.L. Charng, T. Gambin, E. Karaca, G. Mirzaa, W. Wiszniewski, H. Sandoval, N.A. Haelterman, B. Xiong, et al. 2014. A drosophila genetic resource of mutants to study mechanisms underlying human genetic diseases. *Cell.* 159:200–214. https://doi.org/10.1016/j.cell.2014.09.002

Yan, Y., N. Denef, C. Tang, and T. Schüpbach. 2011. Drosophila PI4KIIIalpha is required in follicle cells for oocyte polarization and Hippo signaling. *Development.* 138:1697–1703. https://doi.org/10.1242/dev.059279

Yu, J., and D. Pan. 2018. Validating upstream regulators of Yorkie activity in Hippo signaling through *scalloped*-based genetic epistasis. *Development.* 145:dev157545. https://doi.org/10.1242/dev.157545

Yue, L., and A.C. Spradling. 1992. hu-li tai shao, a gene required for ring canal formation during Drosophila oogenesis, encodes a homolog of adducin. *Genes Dev.* 6:2443–2454. https://doi.org/10.1101/gad.6.12b.2443

Zheng, Y., and D. Pan. 2019. The Hippo signaling pathway in development and disease. *Dev. Cell.* 50:264–282. https://doi.org/10.1016/j.devcel.2019.06.003

Supplemental material

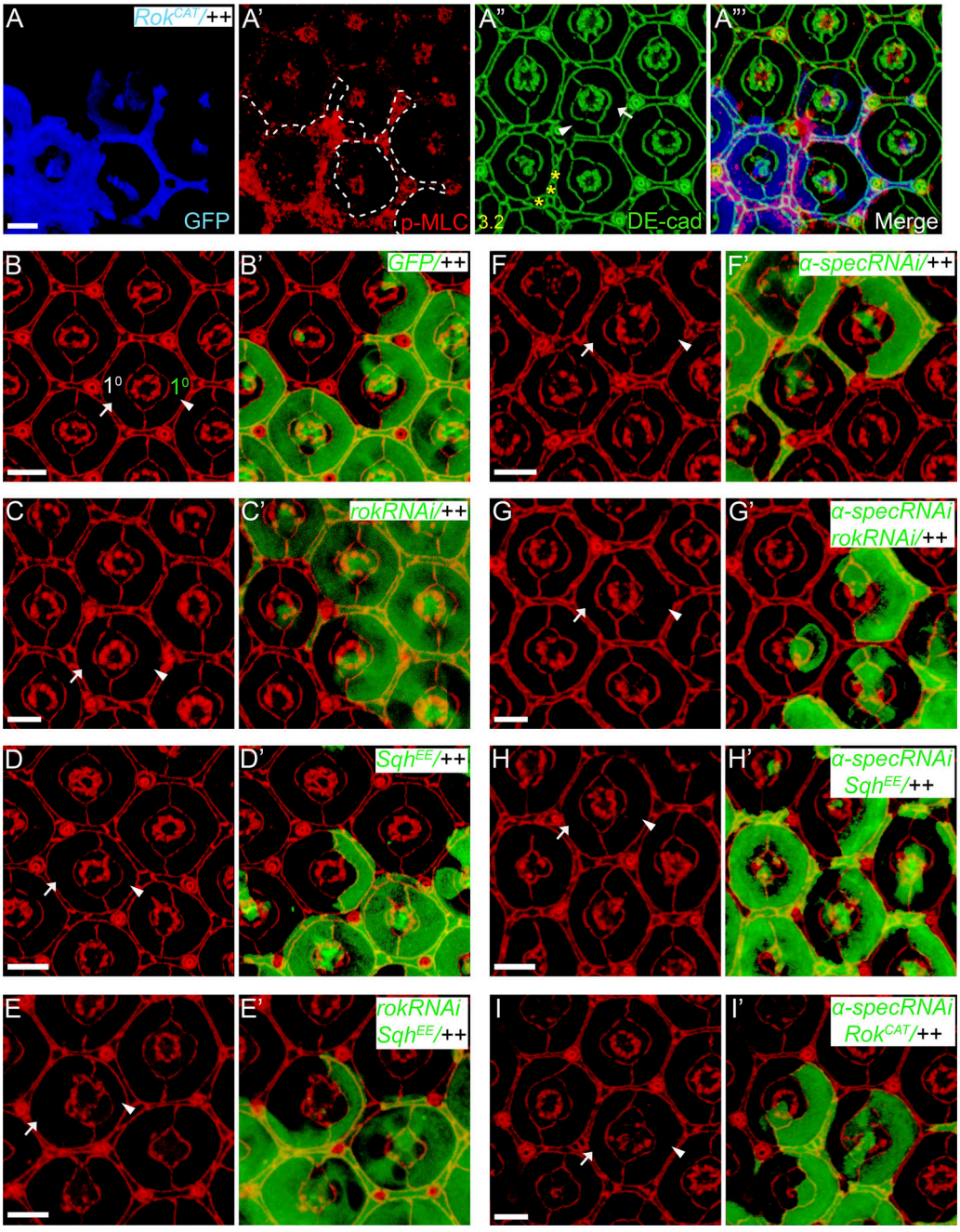

Figure S1. **Further analysis of the coupling between cell shape and myosin II activity in wild-type and spectrin mutant PECs.** All images are z-projections at AJs. Pupal eye discs containing GFP-positive MARCM clones of the indicated genotypes were stained for p-MLC (red) and DE-cad (green) in A–A''' or DE-cad (red) in B–I'. Arrowheads indicate mutant 1° PEC and arrows indicate wild-type 1° PEC from the same mosaic ommatidium. PECs with Rok^{CAT} overexpression show increased p-MLC and decreased apical size compared with wild-type PECs (compare arrow and arrowhead in A''). Also note the extra interommatidial cells (yellow asterisks in A'') in Rok^{CAT} overexpression clones. 20 ommatidia were used for counting interommatidial cells, and the number on the lower left in A'' indicates the number of extra cells per cluster. See Fig. 1 H for quantification of apical area of 1° PEC analyzed in A–I. Scale bars, 5 µm.

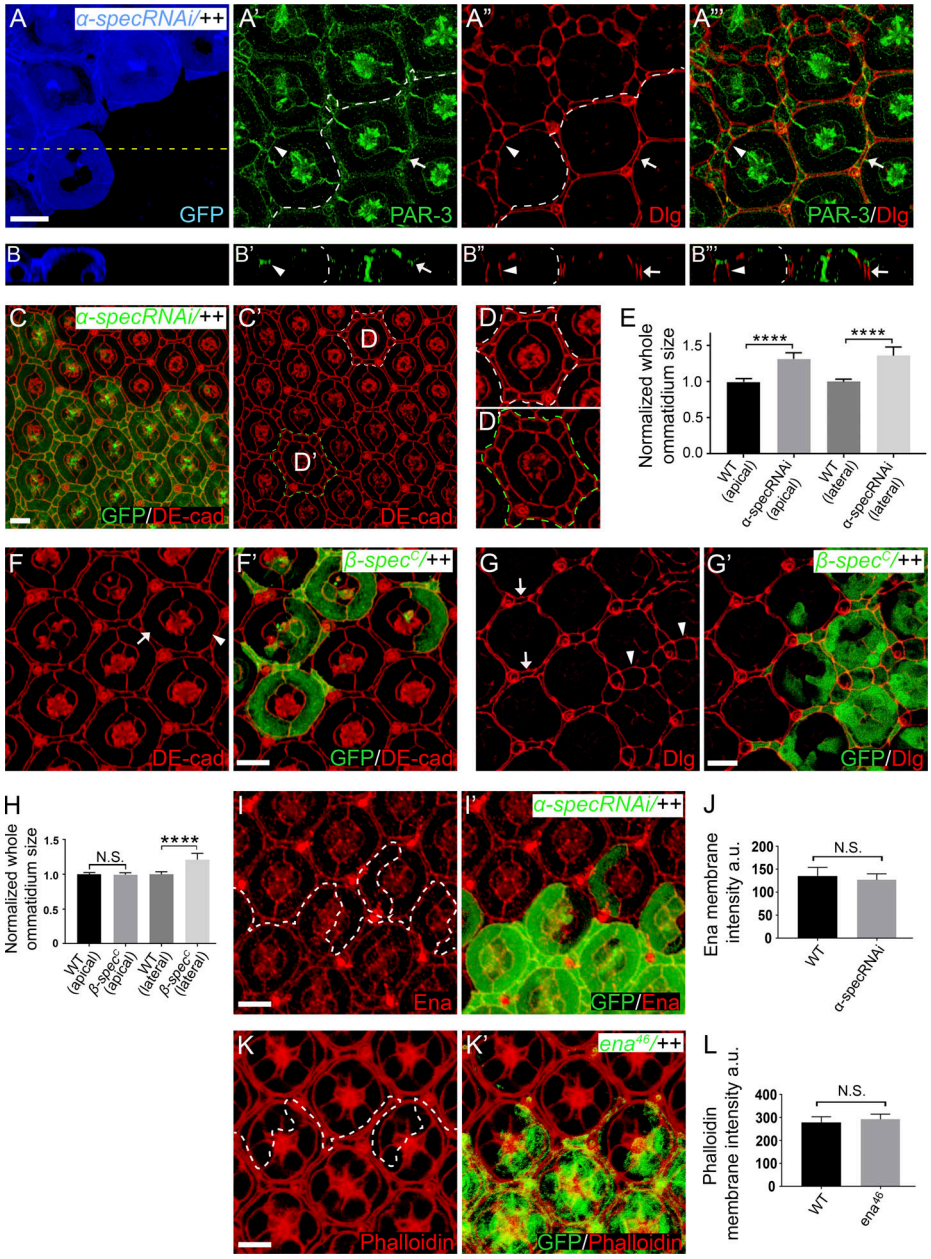

Figure S2. **Analysis of ommatidia size, cell polarity, and Ena expression/function in pupal retina. (A–B"')** A pupal eye disc containing GFP-positive MARCM clones with *α-spec* RNAi was stained for PAR-3 (green) and Dlg (red), which mark the apical and lateral domain of epithelia cells, respectively. **(B–B"')** A vertical section shown through the eye disc in A–A"' in which the position of the vertical section is indicated by a straight dotted line in A. A' and A" show z-projections around cell apical and lateral plane, respectively. Note the normal distribution of PAR-3 and Dlg in *α-spec* mutant PECs (arrowheads) compared with wild-type PECs (arrows). Also note *α-spec* mutant PECs exhibit increased lateral areas than wild-type cells (compare arrowheads and arrows in A" and B"). Quantification of ommatidium size at lateral position is shown in E. **(C–D')** A pupal eye disc containing GFP-positive MARCM clones with *α-spec* RNAi was stained for DE-cad. D and D' are magnified view of the dashed-line circled wild-type and mutant ommatidia in C'. Note that *α-spec* mutant ommatidium (green label in C' and D') exhibit increased apical size compared with wild-type ommatidium (white label in C' and D). Quantification of ommatidium size at apical position is shown in E. **(E)** Normalized mean ommatidium size at apical and lateral position for the indicated genotypes. Data are means ± SEM ($n \geq 15$ ommatidia, representative of five animals). ****, $P < 0.0001$. **(F–G')** Pupal eye discs containing GFP-positive *β-spec*^{C} mutant MARCM clones were stained for DE-cad (red, in F and F'), or Dlg (red, in G and G'). *β-spec*^{C} mutant PECs (arrowhead in F) have similar apical size as wild-type PECs (arrow in F) but exhibit increased lateral size (arrowheads in G) compared with wild-type PECs (arrows in G). Quantification of ommatidium apical and lateral size is shown in H. **(H)** Normalized mean ommatidium apical and lateral size for the indicated genotypes. Data are means ± SEM ($n \geq 15$ ommatidia, representative of five animals). ****, $P < 0.0001$. N.S., no significance. **(I and I')** A pupal eye disc containing GFP-positive MARCM clones with *α-spec* RNAi was stained for Ena (red), showing similar Ena protein level and localization inside and outside the mutant clones. Quantification of Ena membrane intensity is shown in J. **(J)** Mean Ena membrane intensity analyzed in I. Data are means ± SEM ($n \geq 20$ cells, representative of five animals). N.S., no significance. **(K and K')** A Triton X-100–permeabilized pupal eye disc containing GFP-positive *ena*^{46} mutant MARCM clones was stained for phalloidin (red). Note the similar cortical F-actin level inside and outside the mutant clones. Quantification of phalloidin membrane intensity is shown in L. **(L)** Mean phalloidin membrane intensity analyzed in K. Data are means ± SEM ($n \geq 20$ cells, representative of five animals). Scale bars, 5 µm. N.S., no significance.

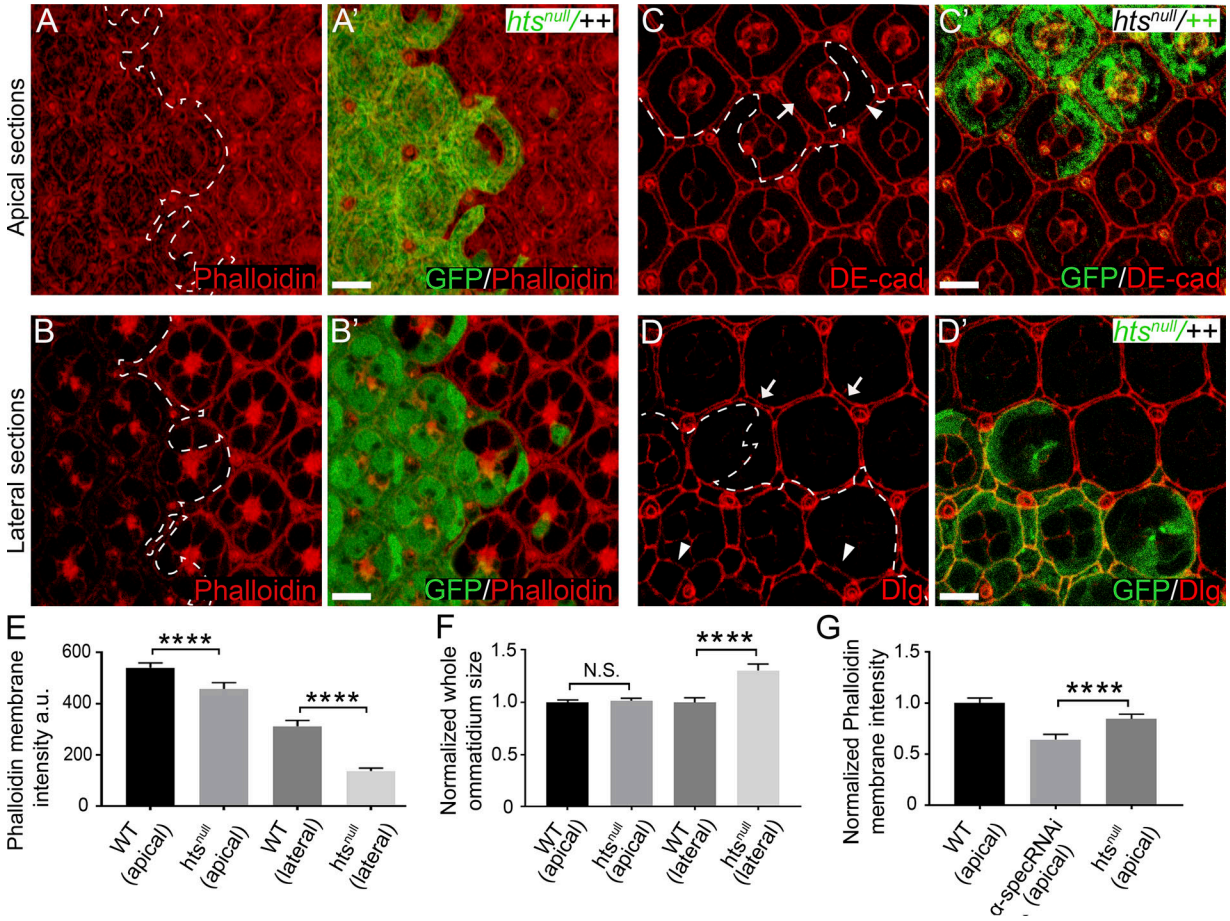

Figure S3. **Analysis of cortical F-actin and cell shape in *hts*^{null} mutant PECs. (A–B')** A Triton X-100–permeabilized pupal eye disc containing GFP-positive *hts*^{null} MARCM clones was stained for phalloidin. A and A' and B and B' show z-projections at apical and lateral position, respectively. Note the reduced cortical F-actin level in *hts*^{null} mutant PECs in both apical and lateral membrane compared with wild-type PECs. Quantification of phalloidin membrane intensity is shown in E. **(C–D')** Pupal eye discs containing GFP-negative *hts*^{null} mutant clones (C and C') or GFP-positive *hts*^{null} MARCM clones (D and D') were stained for DE-cad (red, in C and C') or Dlg (red, in D and D'). *hts*^{null} mutant PECs (arrowhead in C) have similar apical size as wild-type PECs (arrow in C) but exhibit increased lateral size (arrowheads in D) compared with wild-type PECs (arrows in D). Quantification of ommatidium apical and lateral size is shown in F. **(E)** Mean phalloidin membrane intensity of *hts*^{null} mutant PECs at the indicated apical-basal position analyzed in A–B. Note the decrease of phalloidin membrane intensity in both apical and lateral domains. Data are means ± SEM ($n \geq 20$ cells, representative of five animals). ****, $P < 0.0001$. **(F)** Normalized mean ommatidium apical and lateral size analyzed in C–D. Data are means ± SEM ($n \geq 15$ ommatidia, representative of five animals). ****, $P < 0.0001$. N.S., no significance. **(G)** Normalized mean apical membrane phalloidin intensity in PECs of the indicated genotypes. Note the higher apical cortex F-actin level in *hts*^{null} mutant PECs compared with *α-spec* RNAi PECs. ****, $P < 0.0001$. Scale bar, 5 µm.

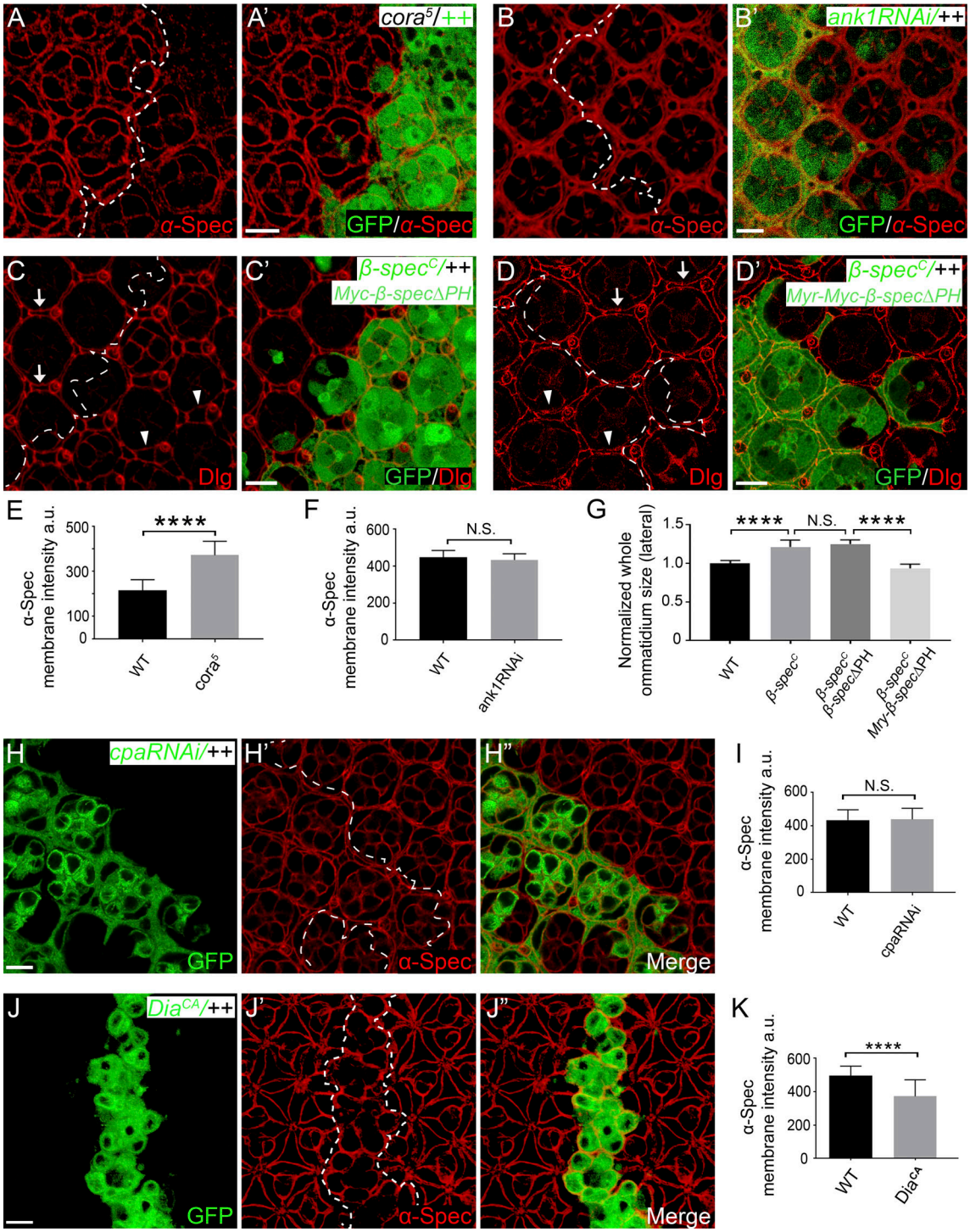

Figure S4. **Analysis of cortical α-Spec level in different genetic background and the importance of the PH domain of β-Spec in cell shape determination.** All images are z-projections at lateral position. **(A and A')** A pupal eye disc containing GFP-negative *cora*^{5} mutant clones was stained for α-Spec. Note the increased cortical α-Spec level in the mutant PECs. Quantification of α-Spec membrane intensity is shown in E. **(B and B')** A pupal eye disc containing GFP-positive MARCM clones with *ank1* RNAi was stained for α-Spec. Note the normal cortical α-Spec level in *ank1* mutant PECs. Quantification of α-Spec membrane intensity is shown in F. **(C–D')** Pupal eye discs containing GFP-positive *β-spec*^{C} mutant MARCM clones expressing β-SpecΔPH (C and C') or Myr-β-SpecΔPH (D and D') were stained for Dlg. Myr-β-SpecΔPH, but not β-SpecΔPH, rescued the cell expansion phenotype of *β-spec*^{C} mutant PECs. Arrows mark wild-type PECs and arrowheads mark *β-spec* mutant PECs expressing the indicated β-Spec transgene. Quantification of ommatidium lateral size is shown in G. **(E and F)** Mean α-Spec membrane intensity in PECs analyzed in A–B. Data are means ± SEM ($n \geq 20$ cells, representative of five animals). ****, $P < 0.0001$. N.S., no significance. **(G)** Normalized mean ommatidium lateral size analyzed in C–D. Data are means ± SEM ($n \geq 15$ ommatidia, representative of five animals). ****, $P < 0.0001$. N.S., no significance. **(H–K)** Pupal eye discs containing GFP-positive MARCM clones with *cpa* RNAi (H–H") or Dia^{CA} overexpression (J–J") were stained for α-Spec (red). Cortical α-Spec level remained unchanged in *cpa* RNAi clones or decreased in Dia^{CA} overexpression clones. Mean α-Spec membrane intensity is shown in I–K. Data are means ± SEM ($n \geq 20$ cells, representative of five animals). ****, $P < 0.0001$. Scale bars, 5 µm. N.S., no significance.

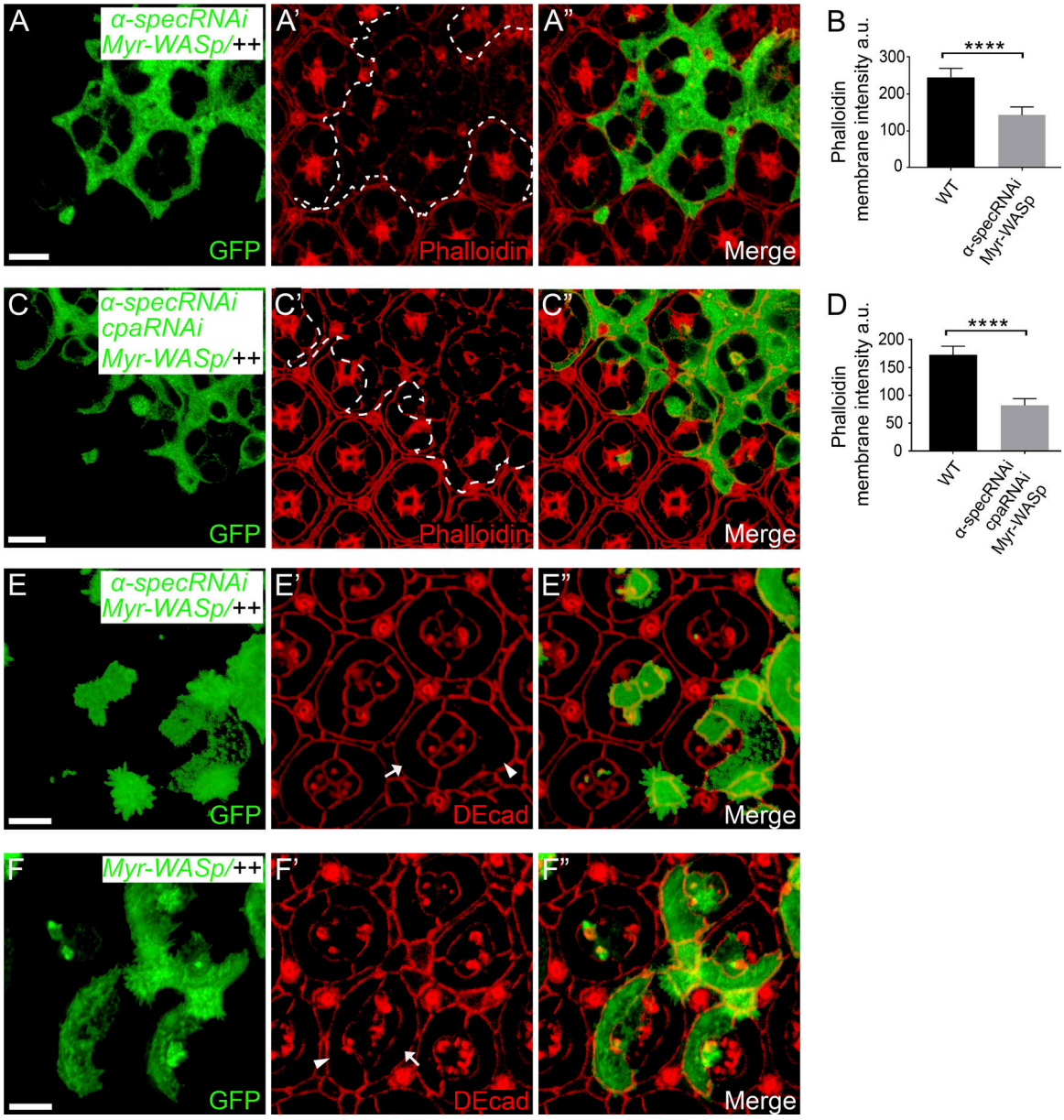

Figure S5. **Myr-WASp overexpression did not rescue the cortical F-actin and cell shape defects in spectrin mutant PECs.** The z-projections at lateral domain (A and C) and z-projections at AJs (E–F). **(A–A")** A Triton X-100–permeabilized pupal eye disc containing GFP-positive MARCM clones with *α-spec* RNAi and Myr-WASp overexpression was stained for phalloidin. Note the decreased cortical F-actin level in the mutant clones. Quantification of phalloidin membrane intensity is shown in B. **(B)** Mean phalloidin membrane intensity analyzed in A–A". Data are means ± SEM ($n \geq 20$ cells, representative of five animals). ****, $P < 0.0001$. **(C–C")** A Triton X-100–permeabilized pupal eye disc containing GFP-positive MARCM clones with *cpa/α-spec* double RNAi and Myr-WASp overexpression was stained for phalloidin. Note the decreased cortical F-actin level in the mutant clones. Quantification of phalloidin membrane intensity is shown in D. **(D)** Mean phalloidin membrane intensity analyzed in C–C". Data are means ± SEM ($n \geq 20$ cells, representative of five animals). ****, $P < 0.0001$. **(E–F")** Pupal eye discs containing GFP-positive MARCM clones with *α-spec* RNAi and Myr-WASp overexpression (E–E") or with Myr-WASp overexpression only (F–F") were stained for DE-cad to reveal cell shape. Note the increased apical area of 1° PEC with *α-spec* RNAi and Myr-WASp overexpression (arrowhead in E') compared with wild-type 1° PEC (arrow in E') in the same mosaic ommatidium. Also note that Myr-WASp overexpression alone did not affect apical area of 1° PEC (compare arrowhead and arrow in F'). Scale bars, 5 µm.